MODIFIED NUMERICAL METHOD FOR THIN FILM THERMAL CONDUCTIVITY CALCULATION WITH MICRO-RAMAN SPECTROSCOPY

by

Taher Meydando

B.S., Mechanical Engineering, Urmia University of Technology, 2018

Submitted to the Institute for Graduate Studies in
Science and Engineering in partial fulfillment of
the requirements for the degree of
Master of Science

Graduate Program in Mechanical Engineering

Boğaziçi University

2021

DEDICATION

To Faezeh, Mom, Dad, and Mahdi.

ACKNOWLEDGEMENTS

I would first like to express my deepest appreciation to my dear supervisor, Dr. Nazlı Dönmezer for her encouragement and continuous support throughout my research studies. Her guidance and advice carried me though all the stages of writing my thesis. Without her accompaniment and expertise, this study would indeed not have been successful. I would also like to thank my committee members, Dr. Nuri Ersoy and Dr. Selçuk Yerci for reviewing my work, giving helpful advice, and sharing their helpful criticism. A debt of gratitude is also owed to The Scientific and Technological Research Council of Turkey (TÜBİTAK) for their financial support with grant number 119F049 during my study.

I cannot leave Boğaziçi without mentioning the support of my dear friends Amir, Aras, Onurcan, Haluk, Mertcan, İlke, Emine, and Canberk. They did not hesitate for a while to help me when I was a new international student in Turkey. I would also like to thank all MiNThLab group members for their insightful suggestions during our weekly meetings and their contribution to my graduate studies.

Finally, I want to give my special thanks to the love of my life Faezeh and my family as a whole for their constant support and understanding during this difficult journey of my life. I am extremely grateful to them for their love, prayers, and sacrifices for preparing me for my future.

ABSTRACT

MODIFIED NUMERICAL METHOD FOR THIN FILM THERMAL CONDUCTIVITY CALCULATION WITH MICRO-RAMAN SPECTROSCOPY

Thin film materials have recently drawn a great attention for their wide range of applications in nano- and micro-scale devices. To overcome thermal issues associated with these devices, thin film materials must be thermally characterized since they do not have the same thermal properties as their bulk counterparts. Various analytical and experimental techniques are used to find thin film thermal conductivities. Micro-Raman spectroscopy is a preferred technique among other optical thermal conductivity measurement techniques due to its non-destructive and non-contact nature. However, the thermal size effects originating from both localized heat generation from Raman laser and phonon scattering at boundaries cause erroneous estimation of the thermal conductivities with the current methods. In this study, the gray phonon Boltzmann transport equation (BTE) is used to simulate the real conditions during the Raman experiment. Thermal conductivities from the developed virtual Raman experiment are then compared with a simple slab model in which the deduction of thermal conductivity in sub-micron thicknesses is calculated using the reduced BTE heat flux through the slab, resulting from phonon directional energy densities. Due to the frequency independence of single phonon mode in the gray BTE model, our method stays ahead of most theoretical methods in calculation time while giving adequate agreement with the literature data. The results show that the results from the developed model are in a good agreement with the slab model results as well as literature values.

ÖZET

MİKRO-RAMAN SPEKTROSKOPİSİ İLE İNCE FİLM TERMAL İLETKENLİK HESAPLAMASI İÇİN MODİFİYE SAYISAL YÖNTEM

İnce film malzemeleri son zamanlarda nano ve mikro ölçekli cihazlarda geniş uygulama yelpazesi nedeniyle büyük ilgi görmüştür. Bu cihazlarla ilgili termal sorunların üstesinden gelmek için, ince film malzemeleri, toplu muadilleriyle aynı termal özelliklere sahip olmadıklarından termal olarak karakterize edilmelidir. İnce film termal iletkenliklerini bulmak için çeşitli analitik ve deneysel teknikler kullanılır. Mikro-Raman spektroskopisi, tahribatsız ve temassız yapısı nedeniyle diğer optik termal iletkenlik ölçüm teknikleri arasında tercih edilen bir tekniktir. Ancak hem Raman lazerden lokalize ısı oluşumundan hem de sınırlarda fonon saçılmasından kaynaklanan termal boyut etkileri, mevcut yöntemlerle termal iletkenliklerin hatalı tahmin edilmesine neden olmaktadır. Bu çalışmada, Raman deneyi sırasındaki gerçek koşulları simüle etmek için gri fonon Boltzmann taşıma denklemi (BTE) kullanılmıştır. Geliştirilen sanal Raman deneyinden elde edilen ısıl iletkenlikler, daha sonra, mikron altı kalınlıklarda ısıl iletkenliğin çıkarılmasının, fonon yönlü enerji yoğunluklarından kaynaklanan levha boyunca azaltılmış BTE ısı akısı kullanılarak hesaplandığı basit bir levha modeli ile karşılaştırılır. Gri BTE modelinde tek fonon modunun frekans bağımsızlığı nedeniyle, yöntemimiz literatür verileriyle yeterli uyum sağlarken hesaplama süresinde çoğu teorik yöntemin önünde kalmaktadır. Sonuçlar, geliştirilen modelden elde edilen sonuçların, slab model sonuçları ve literatür değerleri ile uyumlu olduğunu göstermektedir.

TABLE OF CONTENTS

DEDICATION……iii

ACKNOWLEDGEMENTS……iv

ABSTRACT……v

ÖZET……vi

LIST OF FIGURES……ix

LIST OF TABLES……xii

LIST OF SYMBOLS……xiii

LIST OF ABBREVIATIONS……xv

1. INTRODUCTION 1

1.1. Thin Films in Microelectronic Applications 1

1.2. Thermal Problems of Microelectronics 2

1.3. Thin Film Thermal Conductivity 3

1.3.1. Theoretical Methods 5

1.3.2. Experimental Methods 5

1.4. Micro-Raman Thermal Conductivity Measurement 6

1.5. Size Effects in Micro-Raman Thermal Conductivity Measurements 9

2. MOTIVATION 10

3. NUMERICAL SOLUTION OF THE PHONON BOLTZMANN TRANSPORT EQUATION 11

3.1. Angular Discretization 12

3.2. Spatial Discretization 15

4. MODELING THE SIZE EFFECTS - PHONON BTE MODEL 18

4.1. Slab Model 19
4.2. Model of the Experiment (Virtual Experiment) 29
4.2.1. Grid Study 33
4.2.2. Domain Size Study (Boundary effects) 34
4.2.3. Results 36
4.3. Conclusions 43
5. ERROR ANALYSIS OF CONVENSIONAL COMPLEMENTARY MODEL 44
5.1. Conclusions 48
6. CONCLUSIONS AND FUTURE WORK DIRECTIONS 49
6.1. Conclusions 49
6.2. Future Work Directions 49
REFERENCES 51
APPENDIX A: COPYRIGHT PERMISSIONS 59

LIST OF FIGURES

Figure 1.1. Thin-film transistor cross section on flexible plastic substrate [7]. 1

Figure 1.2. Device structure of InGaN/GaN LED epitaxial and transmission electron microscopy image of 70 nm MgO film in the inset [8]. 2

Figure 1.3. Cross sectional view of formed thermal hotspot in operating AlGaN/GaN HEMT. Reprinted by permission from AIP Publishing [11]. License number: 5237020572679. 3

Figure 1.4. (a) Diffusive, (b) ballistic, and (c) quasi-ballistic heat transport regimes across thin films with different MFP to characteristic length ratios. Reprinted by permission from AIP Publishing [16]. License number: 5237020398417. 4

Figure 1.5. Schematic of the simulation cell for thermal conductivity calculation with molecular dynamics study. Reprinted by permission from RSC Publishing [23]. License number: 1182888-1 5

Figure 1.6. Micro-Raman thermometry experiment schematic [29]. 6

Figure 1.7. Types of scattered light during a Raman thermometry experiment and energy level of each scattered light [31]. 7

Figure 1.8. (a) Raman spectra for different temperatures and (b) Raman shift value in terms of measured temperature. Reprinted by permission from AIP Publishing [32]. License number: 5237030605177 8

Figure 3.1. Angular discretization of phonon BTE with discrete ordinates method. 14

Figure 3.2. Spatial discretization of phonon BTE 2D domain with finite volume method.. 15

Figure 3.3. Spatial discretization of phonon BTE 3D domain with finite volume method.. 16

Figure 4.1. The workflow of simulations in this study. 18

Figure 4.2. Schematic of the 2D slab model, applied boundary conditions and model parameters. 19

Figure 4.3. Fourier temperature contour of a 1µm Si thin film with 10mm height 20

Figure 4.4. BTE *t*emperature distribution in a 1µm Si thin film with 10mm height. 20

Figure 4.5. Temperature contour of a 1µm Si thin film with 1µm height. 22

Figure 4.6. Non-dimensional thermal conductivity of 1µm Si thin film derived from central and bottom heat fluxes in terms of height. 23

Figure 4.7. BTE and Fourier temperature profiles of the 1µm Si thin film at $y=l_y/2$. 24

Figure 4.8. Thickness dependent thermal conductivity of Si derived from the slab model validated by results of Lingping *et al.* [39], Hua *et al.* [40], and Chengyun *et al.* [41]..... 25

Figure 4.9. Thickness dependent thermal conductivity of GaAs derived from the slab model validated by results of Luo *et al.* [42] and Freedman *et al.* [43]. 26

Figure 4.10. Thickness dependent thermal conductivity of GaN derived from the slab model validated by results Freedman *et al.* [43] and Beechem *et al.* [44]. 26

Figure 4.11. Thickness dependent thermal conductivity of MLG derived from the slab model validated by results of Gholivand and Donmezer [45]..... 27

Figure 4.12. (left) BTE and Fourier temperature profiles of 1µm sample of GaAs, Si, GaN, and MLG and (right) derived thickness-dependent thermal conductivities. 29

Figure 4.13. Schematic of the 3D virtual Raman experiment model with applied boundary conditions and model parameters. 30

Figure 4.14. Gaussian laser beam where ω_0, z_R and $\omega(z)$ are waist radius, Rayleigh range and laser beam radius at distance z Reprinted by permission from Elsevier [55]. License number: 5237030873237 32

Figure 4.15. Grid independence study for the 3D model. 34

Figure 4.16. Length independency study for temperature measurement. 35

Figure 4.17. 3D temperature distribution of (left) Fourier and (right) BTE solutions for a 1μm Si thin film. 36

Figure 4.18. Temperature contour of the Fourier solution on the (left) z-y and (right) x-y plane. 37

Figure 4.19. Temperature contour of the BTE solution on the (left) z-y and (right) x-y plane. 37

Figure 4.20. BTE and Fourier temperature profiles along the (left) radial (x or y) and (right) axial (z) directions of 1μm Si thin film with 10mW laser power. 38

Figure 4.21. Variation of maximum temperature difference between BTE and Fourier for 100 nm and 500 nm Si thin films for laser powers of 10 mW, 50 mW, and 100 mW in the same probing wavelength of 532 nm and waist radius of 362 nm... 39

Figure 4.22. Variation of maximum temperature difference between BTE and Fourier for 100 nm and 500 nm GaN thin films for laser powers of 10 mW, 50 mW, and 100 mW in the same probing wavelength of 532 nm and waist radius of 362 nm. 40

Figure 4.23. Variation of maximum temperature difference between BTE and Fourier for 100 nm and 500 nm GaAs thin films for laser powers of 10 mW, 50 mW, and 100 mW in the same probing wavelength of 532 nm and waist radius of 362 nm. 41

Figure 4.24. Variation of maximum temperature difference between BTE and Fourier for 100 nm and 500 nm MLG thin films for laser powers of 10 mW, 50 mW, and 100 mW in the same probing wavelength of 532 nm and waist radius of 362 nm. 42

Figure 5.1. The workflow of finding thin film thermal conductivity by the virtual Raman experiment and its error using the slab model. 44

Figure 5.2. Nondimensional thermal conductivity of GaAs compared to the results of the slab model. 45

Figure 5.3. Nondimensional thermal conductivity of Si compared to the results of the slab model. 46

Figure 5.4. Nondimensional thermal conductivity of GaN compared to the results of the slab model. 46

Figure 5.5. Nondimensional thermal conductivity of MLG compared to the results of the slab model. 47

Figure 6.1. Workflow of suggested technique for future works. 50

Figure A.1. Copyright permission for Figure 1.1. 59

Figure A.2. Copyright permission for Figure 1.2. 60

Figure A.3. Copyright permission for Figure 1.3. 61

Figure A.4. Copyright permission for Figure 1.4. 64

Figure A.5. Copyright permission for Figure 1.5. 68

Figure A.6. Copyright permission for Figure 1.6. 72

Figure A.7. Copyright permission for Figure 1.7. 73

Figure A.8. Copyright permission for Figure 1.8. 74

Figure A.9. Copyright permission for Figure 4.14. 77

LIST OF TABLES

Table 3.1. Direction cosines and weights of S_4, S_6, and S_8 quadratures [64]..... 13

Table 4.1. Thermal and phonon properties of GaAs, Si, GaN, and MLG materials. 28

Table 4.2. Optical properties of materials at the probing wavelength of 532nm and room temperature (300 K)..... 33

Table 5.1. Error analysis of virtual Raman-based thermal conductivity measurement..... 47

LIST OF SYMBOLS

C	Specific heat
D	Density of states
e	Phonon energy density
e_0	Equilibrium energy density
$e_{i,e}$	Directional phonon energy density at east face
e_i^E	Directional phonon energy density at east centroid
f	Phonon distribution function
$\hbar$	Reduced Planck's constant
k_{bulk}	Bulk thermal conductivity
k_{tf}	Thin film thermal conductivity derived from slab model
k_{tf}^*	Thin film thermal conductivity derived from virtual Raman
l_x	Length of model in x-direction
l_y	Length of model in y-direction
l_z	Length of model in z-direction
q'''	Volumetric heat generation
$\vec{s}_i$	Phonon propagation direction unit vector
$\vec{S}_i$	Direction cosine
t	Time
T	Temperature
T_{ref}	Reference temperature
$\overrightarrow{v_g}$	Phonon group velocity
α	Absorption coefficient
$\Delta\Omega_i$	Directional solid angle
ΔV	Volume of control volume
Δx	Cell spacing in the x-direction

Δy	Cell spacing in the y-direction
Δz	Cell spacing in the z-direction
θ_i	Directional polar angle
Λ	Phonon mean free path
ρ	Reflectance
τ	Phonon relaxation time
ϕ_i	Directional azimuthal angle
ω	Phonon frequency

LIST OF ACRONYMS/ABBREVIATIONS

2D	Two Dimensional
3D	Three Dimensional
AlGaN	Aluminum Gallium Nitride
BTE	Boltzmann Transport Equation
CDS	Central Differencing Scheme
FVDOM	Finite Volume Discrete Ordinates Method
GaAs	Gallium Arsenide
GaN	Gallium Nitride
HEMT	High Electron Mobility Transistor
IC	Integrated Circuits
InGaN	Indium Gallium Nitiride
LED	Light Emitting Diode
LUS	Linear Upwinding Scheme
MD	Molecular Dynamics
MFP	Mean Free Path
MgO	Magnesium Oxide
MLG	Multi-layer Graphene
OLED	Organic Light Emitting Diode
Si	Silicon
TC	Thermal Conductivity
TDTR	Time Domain Thermoreflectance
TEM	Transverse Electromagnetic
TFT	Thin Film Transistor

1. INTRODUCTION

1.1. Thin Films in Microelectronic Applications

Recent advancements in microfabrication technology have made it possible to produce thin films with submicron thicknesses [1]. Fabricated thin films are used in the production of various microelectronic devices such as transistors [2], diodes [3], microprocessors [4], and solar cells [5]. Thin films are the promising parts of transistors which are the most basic components of integrated electronic circuits (ICs) in modern semiconductor electronics [6]. For instance, Figure 1.1 shows the structure of a thin-film transistor cross section which is composed of various thin films with thicknesses ranging from 5 nm to 50 µm. These devices are generally used to switch electrical power or signal. On the other hand, light Emitting Diodes (LEDs) are another most common applications of thin films that are used as visible and infrared light source. An InGaN/GaN LED is shown in Figure 1.2 which also consists of several thin film materials. Therefore, due to wide range of their applications in nano and microstructures, thin films should be thermally characterized in an accurate way.

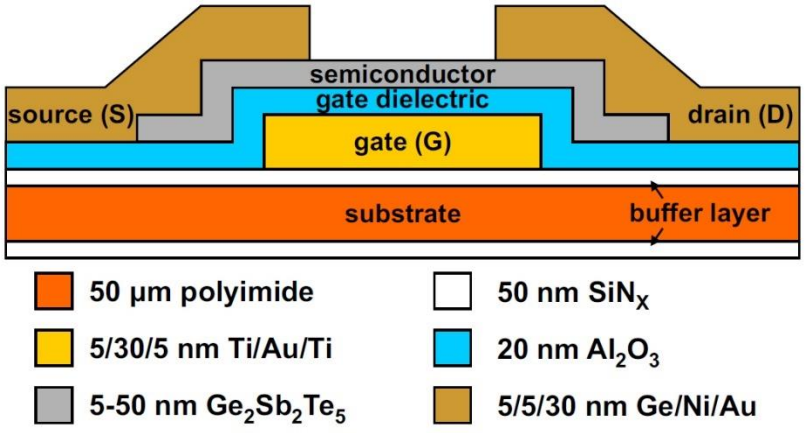


Figure 1.1. Thin-film transistor cross section on flexible plastic substrate [7].

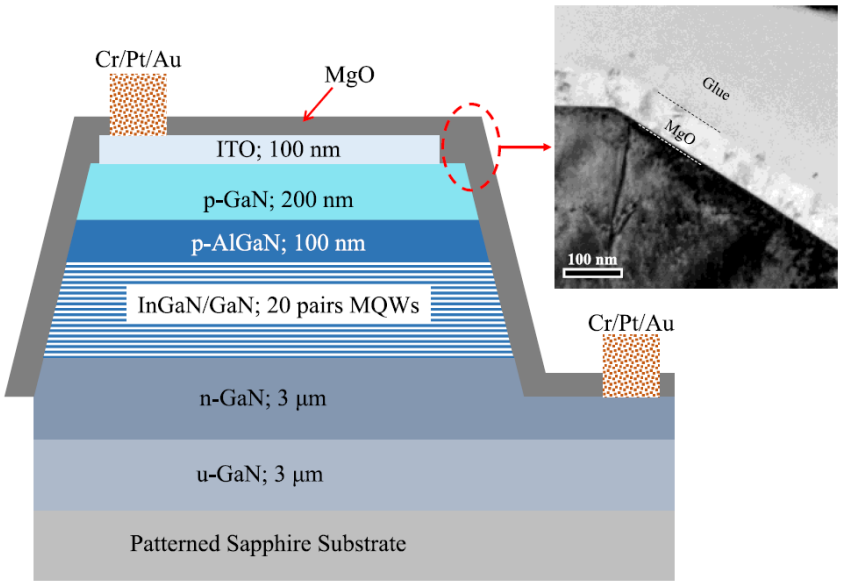


Figure 1.2. Device structure of InGaN/GaN LED epitaxial and transmission electron microscopy image of 70 nm MgO film in the inset [8].

1.2. Thermal Problems of Microelectronics

High temperatures during operation of thin film transistors and high-power LEDs as well as other nano and micro-scale electronic devices may cause degradation in devices. For instance, the hot spot region formed in Figure 1.3 due to accumulation of electrons in the drain side of the gate negatively affects the performance of an AlGaN/GaN HEMT. Therefore, the Joule heating effect causes significant problems in the process of thermal management to maintain maximum temperature under the allowed value [9]. Also there may be nonuniform luminance problems caused by inaccurate characterization of thin film transistors (TFTs) as well as image sticking problems because of organic light emitting diodes (OLEDs) degradation [10]. Therefore, to overcome thermal problems related to thin film devices and to extend their lifetime, their thickness dependent thermal conductivities should be obtained via theoretical or experimental techniques.

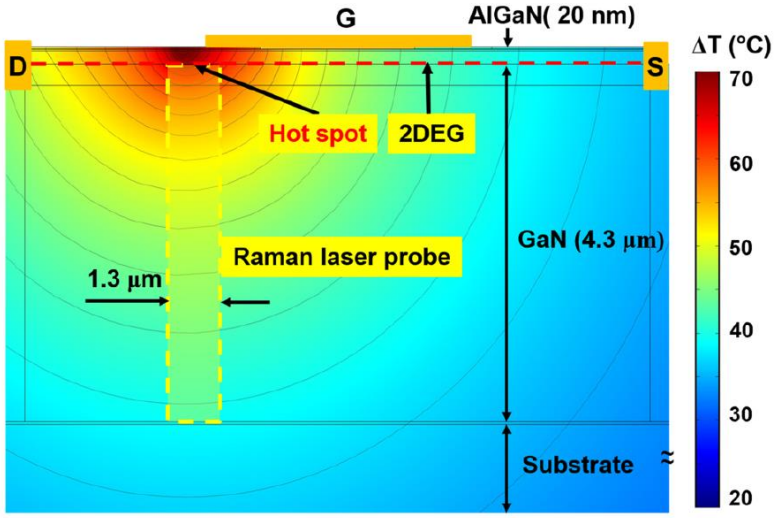


Figure 1.3. Cross sectional view of formed thermal hotspot in operating AlGaN/GaN HEMT. Reprinted by permission from AIP Publishing [11]. License number: 5237020572679.

1.3. Thin Film Thermal Conductivity

Understanding the heat transport phenomena across thin films with thicknesses comparable to or smaller than their mean free path (MFP) which is the distance that phonons can travel before exchanging their energy with other phonons, is a crucial step to calculate their thermal properties. To recognize the appropriate regime for heat transfer in thin films, the Knudsen number is defined as the ratio of phonon mean free path (MFP) to the characteristic length of the problem [12]. Figure 1.4 shows different heat transport regimes for a specified material (same MFP) according to the thickness of the film. Figure 1.4 (a) shows a fully diffusive regime in which almost all phonons are able to complete their MFP before colliding with each other or colliding with boundaries. However, as shown in Figure 1.4 (b), excited phonons at the bottom boundary, become unable to travel a distance equal to their MFP before reaching the top boundary. Therefore, the contribution of phonons to carry the energy from bottom to top, that is said to be the heat flux, reduces significantly [13]. In other words, spatial confinement of heat carriers in thin films results in a notable reduction in the value of layer thermal conductivity which is the relation between the hat flux and temperature gradient through the Fourier law of heat conduction [14]. Finally, Figure 1.4 (c) shows a quasi-ballistic

heat transport regime which happens when the layer thickness is nearly equal to the phonon MFP which includes both of diffusive and ballistic regimes.

Therefore, due to boundary scattering effects associated with ballistic thermal transport in thin films with thicknesses in the range of their mean free path (MFP) and lower, their thermal conductivity is not equal to their bulk counterparts' [15]. For that reason, quantifying the reduced thin film thermal conductivity plays an important role in thermal management and predicting junction temperature of nano and micro-devices consisting of thin films for maintenance purposes. There are various theoretical and experimental techniques for thin film thermal characterization. In this section, some of these methods and their advantages and disadvantages are discussed.

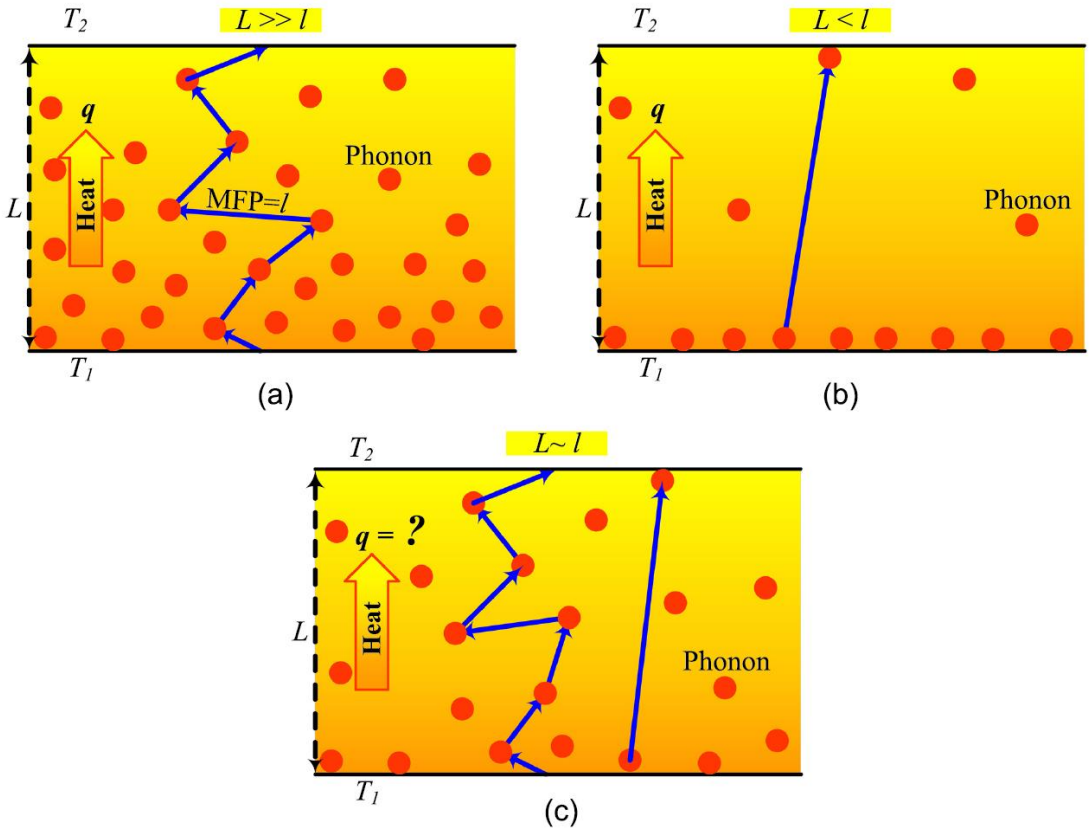


Figure 1.4. (a) Diffusive, (b) ballistic, and (c) quasi-ballistic heat transport regimes across thin films with different MFP to characteristic length ratios. Reprinted by permission from AIP Publishing [16]. License number: 5237020398417.

1.3.1. Theoretical Methods

Theoretical studies are mainly classified into two main categories, atomic-scale and meso-scale methods. Atomic-scale methods include molecular dynamics (MD) simulations [17], ab-initio calculations [18], or non-equilibrium Green's function solutions [19], where meso-scale methods include Boltzmann transport equation [20] and Monte Carlo simulations [21]. Figure 1.5 represents a nonhomogeneous nonequilibrium approach of molecular dynamics. In this approach, a constant heat flux is applied to the system in the x-direction, the resulting temperature gradient is extracted, and thermal conductivity is calculated by the Fourier law in which it is equal to the ratio of heat flux to the temperature gradient [22].

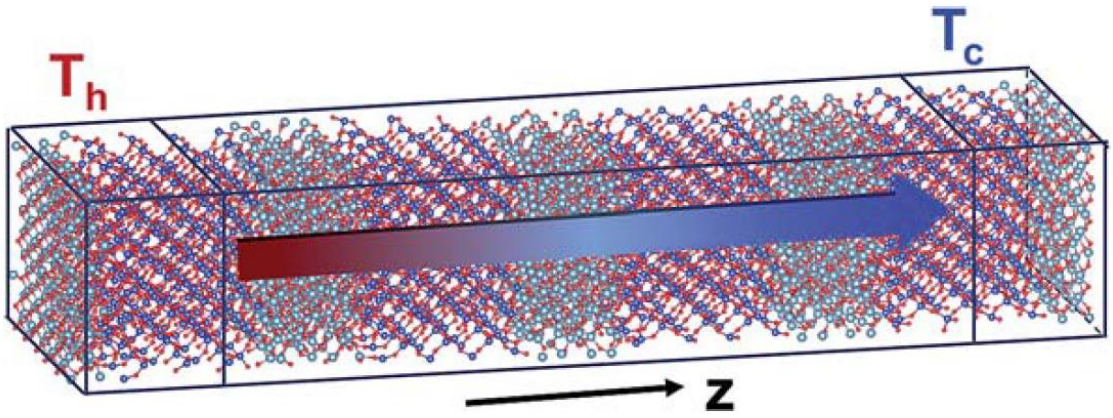


Figure 1.5. Schematic of the simulation cell for thermal conductivity calculation with molecular dynamics study. Reprinted by permission from RSC Publishing [23]. License number: 1182888-1.

1.3.2. Experimental Methods

On the other hand, there are experimental methods to measure thin film thermal conductivity. Among the most prevalent ones, are 3ω, time domain thermoreflectance, frequency domain thermoreflectance, and micro-Raman spectroscopy methods to name a few. A hot strip is put on the specimen which acts as a heater as well as a thermometer in the 3ω

method. The magnitude and phase of the produced harmonic signal as a result of oscillating surface temperature is then used to characterize thermal properties of the underlying thin film sample [24]. A similar trend is followed in time domain thermoreflectance but the difference is that instead of measuring temperature, surface reflectance is measured. In fact, after shining a laser beam onto the surface of specimen, the intensity of reflected light is measured to detect reflectivity that is a function of temperature. Measured reflectivity is matched with a theoretical method to find thermal conductivity [25]. Frequency domain thermoreflectance method is similar to TDTR method with the difference that the excitation laser is pumped with variable frequencies to overcome the problems related to mechanical motion of the probe [26].

1.4. Micro-Raman Thermal Conductivity Measurement

Due to its non-contact and non-destructive nature and no need for microfabrication of the thin film, Raman thermometry method is highly preferred among other experimental methods [27]. Additionally, being able to measure not only cross-plane thermal conductivity but also in-plane thermal conductivity, Raman technique stays ahead of other optical methods [28]. Raman thermometry method includes two main parts including the experiment and complementary thermal modelling sections.

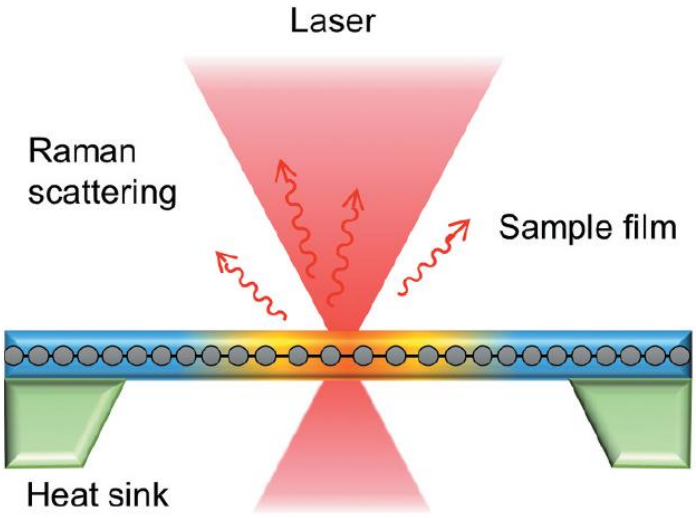


Figure 1.6. Micro-Raman thermometry experiment schematic [29].

In thermal conductivity measurement via micro-Raman experiment, an excitation laser beam is shined onto the sample and the scattered photons are collected as shown in Figure 1.6. In addition to its heating purpose, the laser acts as a probe for the analysis of the scattered light [30]. After absorption of a portion of light source energy, the rest is reflected. The reflected light contains Stokes, anti-Stokes and Rayleigh scattered signals which are all affected by the intensity of interatomic interactions inside the specimen as shown in Figure 1.7. Since Rayleigh scattering is an elastic one and does not carry the information about the molecular vibrations in the sample, the local temperature is measured using Stokes and anti-Stokes Raman scattering signals [31].

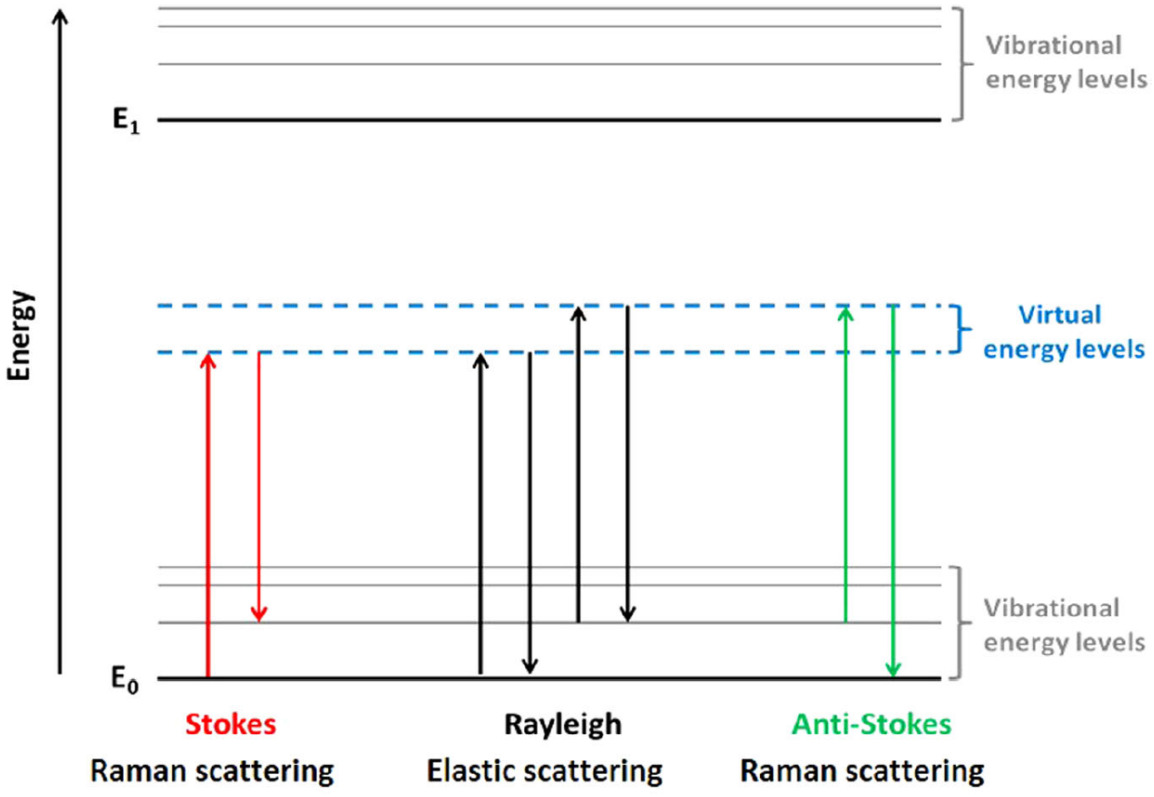


Figure 1.7. Types of scattered light during a Raman thermometry experiment and energy level of each scattered light [31].

After the detection of the scattered light, it is converted to the Raman fingerprint of the material which quantifies the intensity of Raman as a function of Raman shift as shown in Figure 1.8 (a). This test is done for different laser beam powers inducing different Raman fingerprints. The peak position of the Raman spectra differs for any temperature. The relation between the Raman shift peak position and temperature is deduced as shown in Figure 1.8 (b). Therefore, the local temperature can directly be obtained for any Raman spectrum.

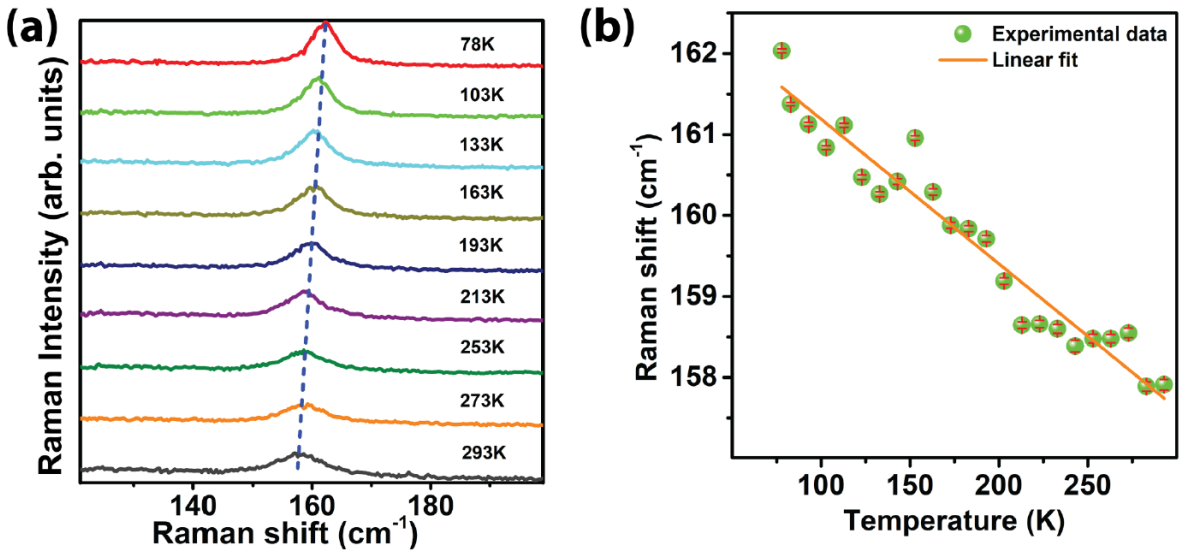


Figure 1.8. (a) Raman spectra for different temperatures and (b) Raman shift value in terms of measured temperature. Reprinted by permission from AIP Publishing [32]. License number: 5237030605177.

In Raman-based thermal conductivity measurement, it is not possible to directly measure thermal conductivity. Instead, local temperature is measured. After finding the hot spot temperature of the sample using the above-mentioned process, a complementary thermal transport model with the same boundary conditions as well as the same heat source according to laser power, probing wavelength, and material optical properties is used to predict the temperature distribution matching the measured temperature [33]. Thermal conductivity giving the best prediction is chosen as the measured thermal conductivity.

1.5. Size Effects in Micro-Raman Thermal Conductivity Measurements

Thermal size effects appear when the heat carriers become unable to transfer energy in their maximum performance. This happens during spatial confinement in thin film materials or when the heat generation region becomes as small as their mean free path. In Rama based thin film thermal conductivity measurement, not only there exists a spatial confinement due to small thin film thickness scales as shown in Figure 1.4, but also a heat generation happening in a very small region due to excitation lasers small diameter. In the conventional thin film thermal conductivity measurement via micro-Raman thermometry, the complementary thermal model is usually a Fourier based one which is not able to take size effects into account.

In order to include localized heating size effects caused by laser beam as well as boundary scattering effects during the Raman thermometry TC measurement, phonon BTE can be used to predict specimen temperature. The initial form of the phonon BTE in terms of phonon statistical distribution function (f) is given as

$$\frac{\partial f}{\partial t} + \overrightarrow{v_g}.\nabla f = \left(\frac{\partial f}{\partial t}\right)_{scatt} + q''' \tag{1.1}$$

where $\overrightarrow{v_g}$ is the phonon group velocity and q''' is the volumetric energy generation if any [34]. The scattering term on the right-hand side of this equation represents the variation of the phonon distribution function due to collisions with other phonons. This term is the main feature of the non-Fourier heat transfer and includes ballistic behavior of phonon transport in small scales. The numerical solution for this equation is introduced in chapter 3.

2. MOTIVATION

The conventional Raman-based thermal conductivity measurement techniques use Fourier-based modeling to predict temperature and therefore thermal conductivity. This research aims to remove the errors in thin thermal conductivity measurement by previous micro-Raman numerical models because of their fully diffusive nature. For this purpose, a modified micro-Raman spectroscopy model is developed which includes size effects associated with boundaries and localized heating by employing a phonon Boltzmann Transport Equation (BTE) to simulate the non-Fourier heat transport in thin films that has not been used previously. In this study Si, GaN, GaAs, and MLG materials are examined since they are promising candidates for thermal characterization due to their wide applications in semiconductor microdevices.

3. NUMERICAL SOLUTION OF THE PHONON BOLTZMANN TRANSPORT EQUATION

Various numerical techniques like Monte Carlo study [35] has been employed to solve Equation (1.1) in the literature. However, this method is not preferred in relatively large domains due to its high computational costs. Therefore, in this study we use a finite volume discrete ordinates method (FVDOM) [36] to solve the gray BTE in which it should be discretized in both spatial and angular coordinates since the phonon energy density is a function of position as well as direction.

To simply apply the phonon BTE to a domain and find the temperature distribution, phonon distribution function is replaced with its energy density function as represented in

$$e(T) = f\hbar\omega D(\omega) \tag{3.1}$$

where e, $\hbar$, ω, and $D(\omega)$ are phonon energy density, reduced Planck's constant, phonon frequency and density of states, respectively. Afterwards, the final steady state phonon BTE under gray relaxation time approximation can be written in terms of phonon energy density in

$$\overrightarrow{v_g}.\nabla f = \frac{e - e_0}{\tau} + q''' \tag{3.2}$$

where τ is the phonon relaxation time which defines the time that phonons travel before they collide with other energy carriers. According to the gray approximation phonons travel in a single group velocity as well as single relaxation time and therefore assumes that phonon properties are frequency-independent [37].

The equilibrium energy density e_0 can be related to lattice temperature using equation

$$e_0 = CT = \sum e_i w_i \tag{3.3}$$

where specific heat C is assumed to be constant and directional weights, w_i are given in Table 3.1.

The kinetic theory is given as

$$k_{bulk} = \frac{1}{3} C v_g^2 \tau = \frac{1}{3} C v_g \Lambda \tag{3.4}$$

which is used to specify phonon properties like group velocity, $\overrightarrow{v_g}$ and relaxation time, τ to be employed in Equation (3.2) where phonon mean free path, Λ is equal to group velocity times relaxation time, $v_g \tau$. This theory relates the material bulk thermal conductivity to its phonon properties.

3.1. Angular Discretization

Unlike Fourier law of heat conduction, phonon BTE needs to be discretized angularly in addition to spatial discretization. At any centroid of control volume, the angular space is discretized into several solid angles so that phonons can propagate in these directions. The number of solid angles is defined by the type of S_N quadrature chosen for discretization. Angularly discretized form of the steady state gray phonon BTE (Equation (3.2)) is rewritten in the form of

$$\vec{s}_i \cdot \nabla v_{gi} e_i = \frac{e_i^0 - e_i}{\tau} + q''' \tag{3.5}$$

where subscript i and $\vec{s}_i$ represent direction and the unit vector along phonon propagation direction. In this equation v_{gi} and e_i are directional phonon group velocity and energy density, respectively. The directional unit vector, $\vec{s}_i$ shown in Figure 3.1 can be written in terms of polar and azimuthal angles as shown in

$$\vec{s}_i = sin(\theta_i) sin(\phi_i) i + sin(\theta_i) cos(\phi_i) j + cos(\theta_i) k \tag{3.6}$$

where i, j, and k are unit vectors along x, y, and z directions, respectively.

Components of directional unit vector (shown in Figure 3.1) for any S_N quadrature can be found in Table 3.1. The number of possible directions for any S_N quadrature can be found by the following formula $N(N+2)$. For instance, in a 3D problem there are 24 possible directions for the S_4 quadrature. However, for a 2D problem there will be 12 possible directions inside half of the sphere. It should be noted that in this case weights (in Table 3.1 must be doubled for the corresponding directions.

Table 3.1. Direction cosines and weights of S_4, S_6, and S_8 quadratures [38].

Quadrature	Direction cosines			Weight
	μ	η	ξ	w
S_4	0.2958759	0.2958759	0.9082483	0.5235987
	0.2958759	0.9082483	0.2958759	0.5235987
	0.9082483	0.2958759	0.2958759	0.5235987
S_6	0.1838670	0.1838670	0.9656013	0.1609517
	0.1838670	0.6950514	0.6950514	0.3626469
	0.1838670	0.9656013	0.1838670	0.1609517
	0.6950514	0.1838670	0.6950514	0.3626469
	0.6950514	0.6950514	0.1838670	0.3626469
	0.9656013	0.1838670	0.1838670	0.1609517
S_8	0.1422555	0.1422555	0.9795543	0.1712359
	0.1422555	0.5773503	0.8040087	0.0992284
	0.1422555	0.8040087	0.5773503	0.0992284
	0.1422555	0.9795543	0.1422555	0.1712359
	0.5773503	0.1422555	0.8040087	0.0992284
	0.5773503	0.5773503	0.5773503	0.4617179
	0.5773503	0.8040087	0.1422555	0.0992284
	0.8040087	0.1422555	0.5773503	0.0992284
	0.8040087	0.5773503	0.1422555	0.0992284
	0.9795543	0.1422555	0.1422555	0.1712359

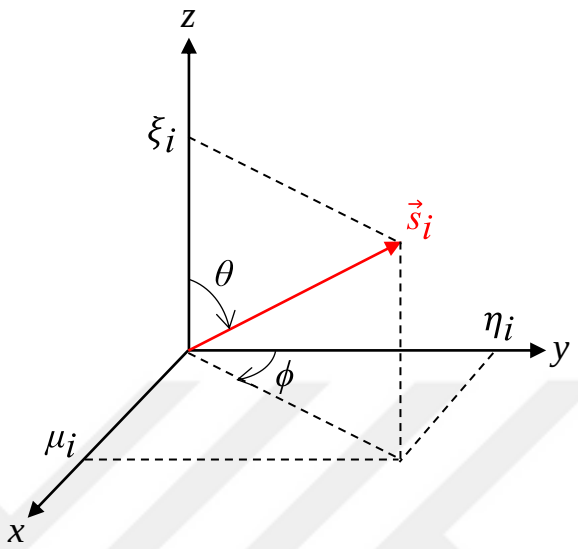


Figure 3.1. Angular discretization of phonon BTE with discrete ordinates method.

Integrating Equation (3.5) over the discrete angular control volume, angularly discretized phonon BTE is rewritten in the form of

$$\vec{S}_i \cdot \nabla v_g e_i = \frac{e_i^0 - e_i}{\tau} \Delta\Omega_i + q''' \Delta\Omega_i \tag{3.7}$$

where the direction cosine $\vec{S}_i$ and directional solid angle $\Delta\Omega_i$ are given in

$$\vec{S}_i = \int_{(\phi_i - \Delta\phi/2)}^{(\phi_i + \Delta\phi/2)} \int_{(\theta_i - \Delta\theta/2)}^{(\theta_i + \Delta\theta/2)} \vec{s}_i \, sin(\theta) d\theta d\phi \tag{3.8}$$

and

$$\Delta\Omega_i = \int_{(\phi_i - \Delta\phi/2)}^{(\phi_i + \Delta\phi/2)} \int_{(\theta_i - \Delta\theta/2)}^{(\theta_i + \Delta\theta/2)} sin(\theta) d\theta d\phi \tag{3.9}$$

where θ and ϕ are polar and azimuthal angles.

The equilibrium energy density and control volume centroid temperature can be calculated through equation

$$4\pi e^0 = C\left(T - T_{ref}\right) = \sum_{i=1}^{N(N+2)} e_i \Delta\Omega_i \tag{3.10}$$

using directional energies and corresponding solid angle. The angular discretization is the same for the 2D and 3D models where it differs in spatial discretization.

3.2. Spatial Discretization

For the spatial discretization of the 2D and 3D phonon BTE, domains are divided into rectangular control volumes as shown in Figures 3.2 and 3.3. Integrating Equation (3.7) over the spatial control volume, that has been integrated over the angular control volume in the previous section, the final form of discretized phonon BTE comes in Equations (3.11) and (3.12) for 2D and 3D problems, respectively.

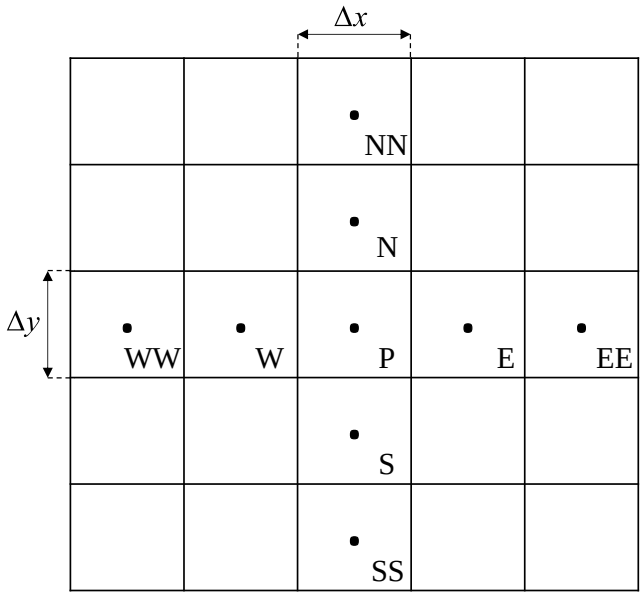


Figure 3.2. Spatial discretization of phonon BTE 2D domain with finite volume method.

The discretized phonon BTE in 2D is given as

$$v_g e_{i,e} \Delta y S_{i,x} - v_g e_{i,w} \Delta y S_{i,x} + v_g e_{i,n} \Delta x S_{i,y} - v_g e_{i,s} \Delta x S_{i,y} = \frac{e^0 - e_i}{\tau} \Delta V \Delta \Omega_i + q''' \tag{3.11}$$

where ΔV is equal to $\Delta x \Delta y$.

On the other hand, the 3D version of fully discretized phonon BTE is given as

$$\begin{aligned} v_g e_{i,e} \Delta y \Delta z S_{i,x} - v_g e_{i,w} \Delta y \Delta z S_{i,x} + v_g e_{i,n} \Delta x \Delta z S_{i,y} \\ - v_g e_{i,s} \Delta x \Delta z S_{i,y} + v_g e_{i,f} \Delta x \Delta y S_{i,z} \\ - v_g e_{i,b} \Delta x \Delta y S_{i,z} = \frac{e^0 - e_i}{\tau} \Delta V \Delta \Omega_i + q''' \end{aligned} \tag{3.12}$$

where ΔV is equal to $\Delta x \Delta y \Delta z$ and $e_{i,e}$, $e_{i,w}$, $e_{i,n}$, $e_{i,s}$, $e_{i,f}$, and $e_{i,b}$ are directional phonon energy densities at east, west, north, south, front, and back faces of the control volume.

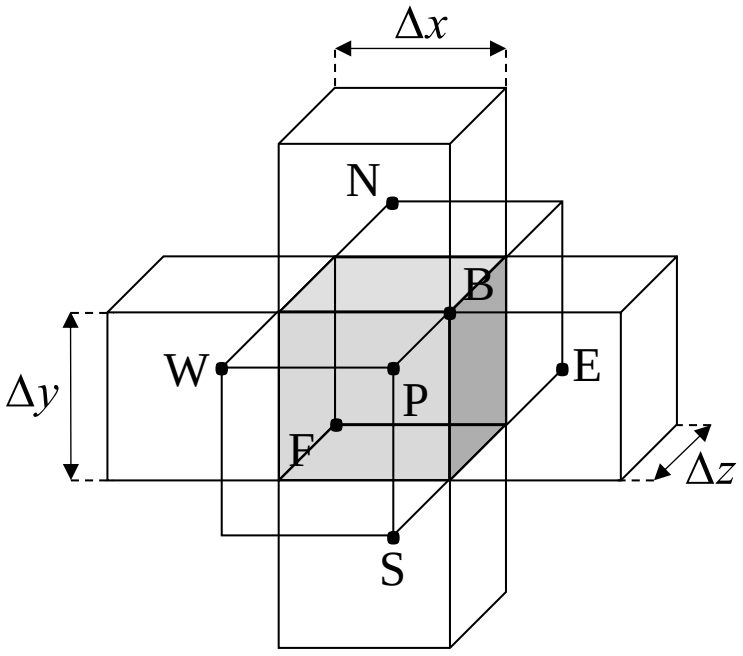


Figure 3.3. Spatial discretization of phonon BTE 3D domain with finite volume method.

To relate facial energy densities to nodal values in 2D version, a Linear Upwind Scheme (LUS) is used in which the direction matters, and they carry the information from where they come. For instance, the directional energy density at east face in the $+x$ direction is

$$e_{i,e}^{+} = e_i^P + \frac{e_i^P + e_i^W}{2} \tag{3.13}$$

while the directional energy density at east face in the $-x$ direction is

$$e_{i,e}^{-} = e_i^E + \frac{e_i^E + e_i^{EE}}{2} \tag{3.14}$$

where the capital superscripts represent cell centroid values as shown in Figure 3.2. The rest of the facial values can be derived accordingly.

For the 3D modeling, a Central Differencing Scheme (CDS) is used to define energy densities on the control volume faces as a function of their value in the control volume centroids. For instance, the east face directional energy density can be found by

$$e_{i,e} = \frac{e_i^P + e_i^E}{2} \tag{3.15}$$

where the capital superscripts represent cell centroid values as shown in Figure 3.3.

4. MODELING THE SIZE EFFECTS - PHONON BTE MODEL

One of the novelties of this study is to use phonon BTE to understand actual thermal behavior of thin films that are examined under micro-Raman thermography. For this purpose, first a slab model is developed to find the correct phonon properties. This model gives accurate phonon characteristics of any material by validating deduced thin film thermal conductivity with literature values. Therefore, a thermal conductivity spectrum is obtained that will be later used to calculate the error in the virtual Raman experiment. A schematic workflow of the current study is given in Figure 4.1. In this chapter, phonon properties of the materials which are not directly available in the literature are defined by validating the deduced thin film thermal conductivity. Therefore, there will be a better understanding from the actual conditions happening during the Raman experiment by resolving the phonon BTE.

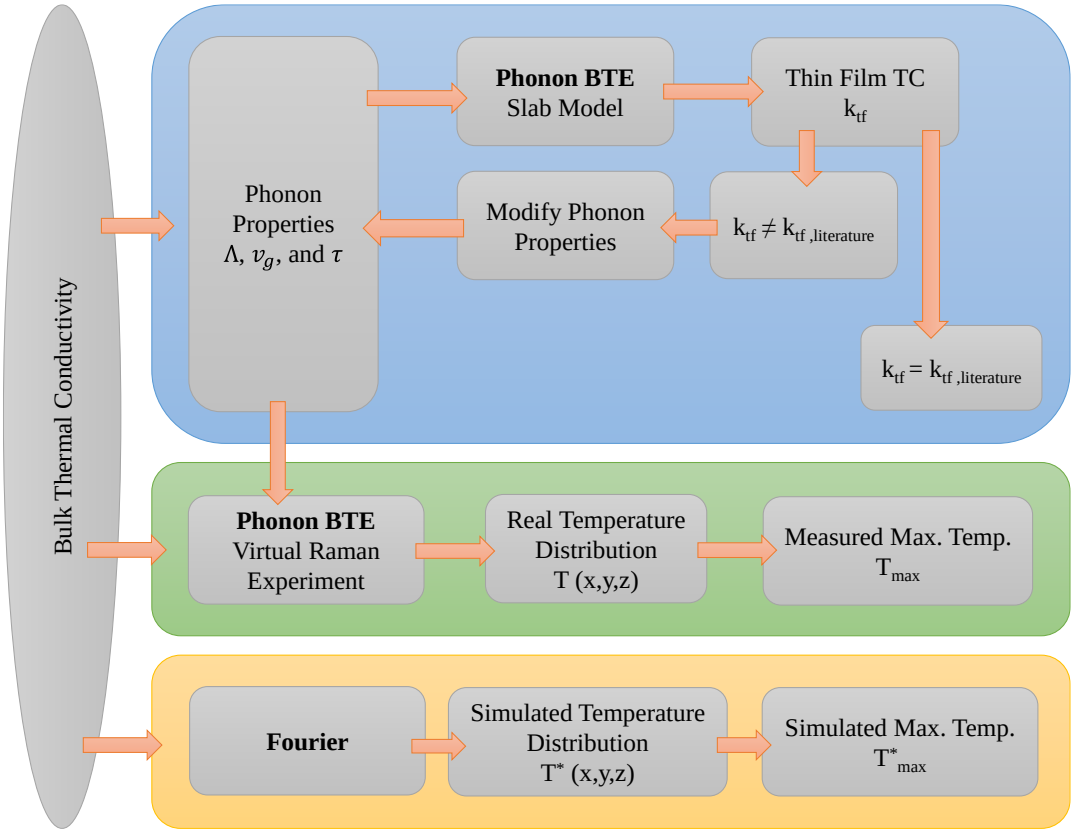


Figure 4.1. The workflow of simulations in this study.

4.1. Slab Model

In order to find the correct phonon properties of the material of interest, a 2D model is developed as shown in Figure 4.2. In this model, to eliminate size effects in y-direction and therefore purely having size effects originating from boundaries in one direction, l_y is long enough to consider infinite length along y-axis as well as infinite length in the direction perpendicular to the x-y plane. Applying zero heat flux boundary condition at top and bottom boundaries as well as different temperatures at left and right boundaries, a uniform heat flux at x-direction is established.

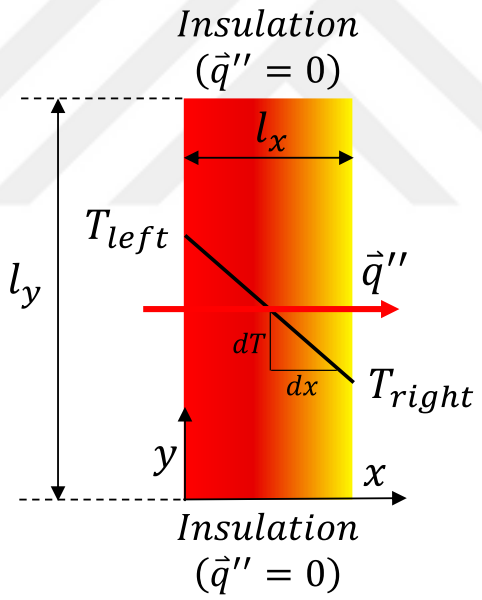


Figure 4.2. Schematic of the 2D slab model, applied boundary conditions and model parameters.

To implement the Fourier law of heat conduction to calculate thin film thermal conductivity as well as phonon BTE initialization, first the problem is solved with the 2D Fourier solvers to obtain the temperature distribution in the slab model as shown in Figure 4.3.

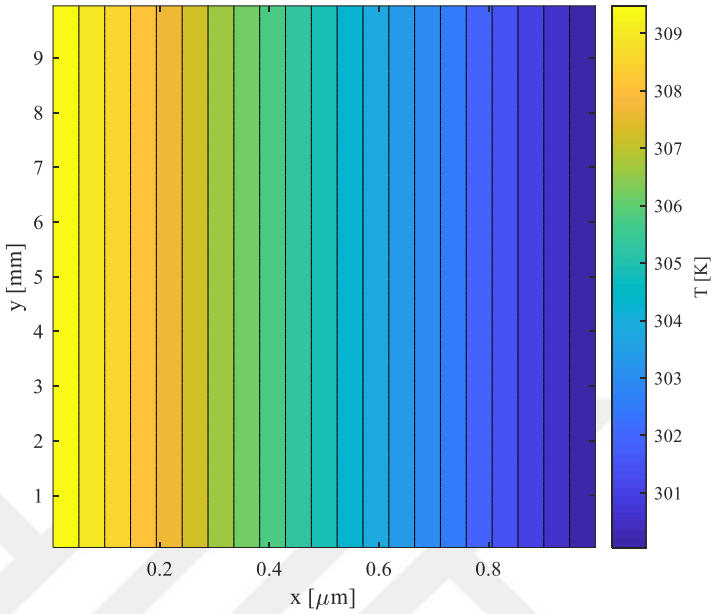


Figure 4.3. Fourier temperature contour of a 1µm Si thin film with 10mm height

On the other hand, phonon properties are guessed to be employed in the BTE solution for the same problem which is free of localized heating size effects (zero heat generation). Phonon properties are co-related to each other by the kinetic theory mentioned in Equation (3.4). Afterwards, BTE temperature distribution is obtained as shown in Figure 4.4.

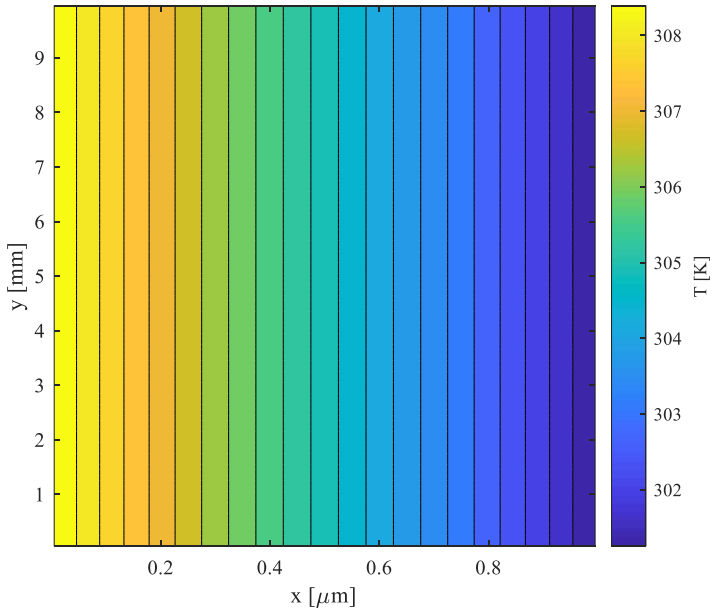


Figure 4.4. BTE *t*emperature distribution in a 1µm Si thin film with 10mm height.

As stated before, temperature profiles of both solutions are extracted at $y=l_y/2$. As shown in Figure 4.7, the slope of BTE temperature profile is lower than the Fourier profile. For any film thickness l_x, the Fourier profile stays the same while due to size effects originating from boundary scattering, temperatures at boundaries tend to tilt towards the average of left and right temperatures. This is because of present size effects originating from boundaries meaning that a set of phonons are incapable of a successful energy exchange along the x-axis inside the thin film.

The slope of the temperature profile shown in Figure 4.7 simply represent the horizontal heat flux. The cumulative reduced heat flux can be calculated from equation

$$\vec{q}'' = q_x''\vec{\imath} + q_y''\vec{j} + q_z''\vec{k} = \sum \vec{v}_i e_i \tag{4.1}$$

using directional energy densities through the BTE solution.

To calculate the reduced thermal conductivity there must be a pure heat transport in the x-direction. According to the 2D nature of the problem, q_z'' is zero. However, due to boundary scattering effects at top and bottom borders for relatively short l_y, q_y'' is not equal to zero. Therefore, to find the suitable length of the model fitting the desired conditions mentioned above, heat flux in the x-direction must be identical at any y distance. For this purpose, a one micrometer thick silicon film is modeled using different heights ranging from 1μm up to 10mm. The temperature profile of BTE solution is shown in Figure 4.5 for a 1μm high sample.

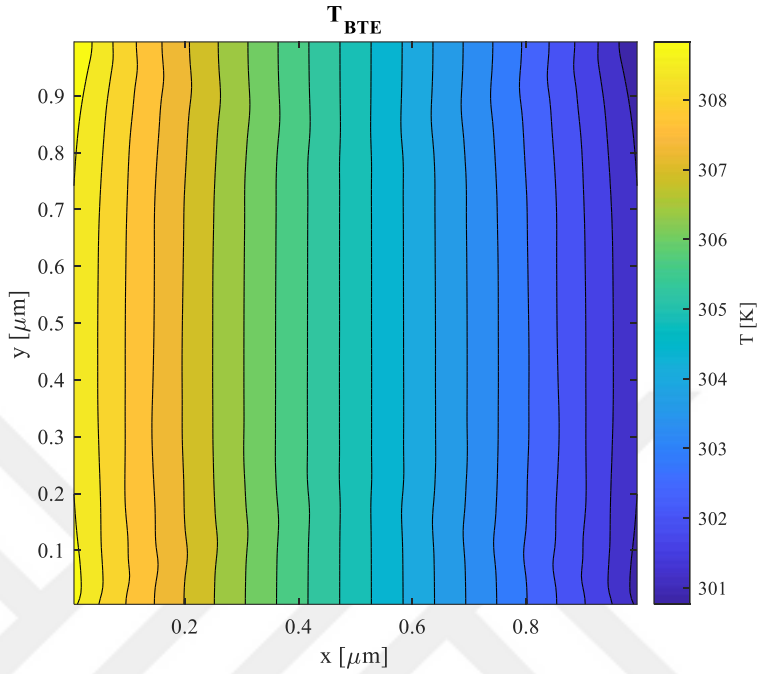


Figure 4.5. Temperature contour of a 1µm Si thin film with 1µm height.

At each step, the difference between maximum Fourier and BTE temperatures are recorded, and it is observed that it is almost the same as the previous step at 10mm height. For each l_y, the reduced BTE heat flux is measured at the center ($y=l_y/2$) and bottom ($y=0$). Reduced thermal conductivities are then calculated according to these heat fluxes that will be explained later. According to this method the difference between calculated thermal conductivities by bottom and central heat fluxes drop down to 0.06% for a height of 10mm as shown in Figure 4.6.

It is understood that slightly curved BTE temperature contour lines in Figure 4.5 for a 1µm×1µm domain become completely vertical for a 1µm×10mm domain shown in Figure 4.4. This inspires us to use a height of at least 10000 times of thickness if we are interested in a semi 1D heat transport. However, it is sufficient to use height of ten times thickness to calculate thermal conductivity employing central ($y=l_y/2$) heat flux in order to avoid longer computational time.

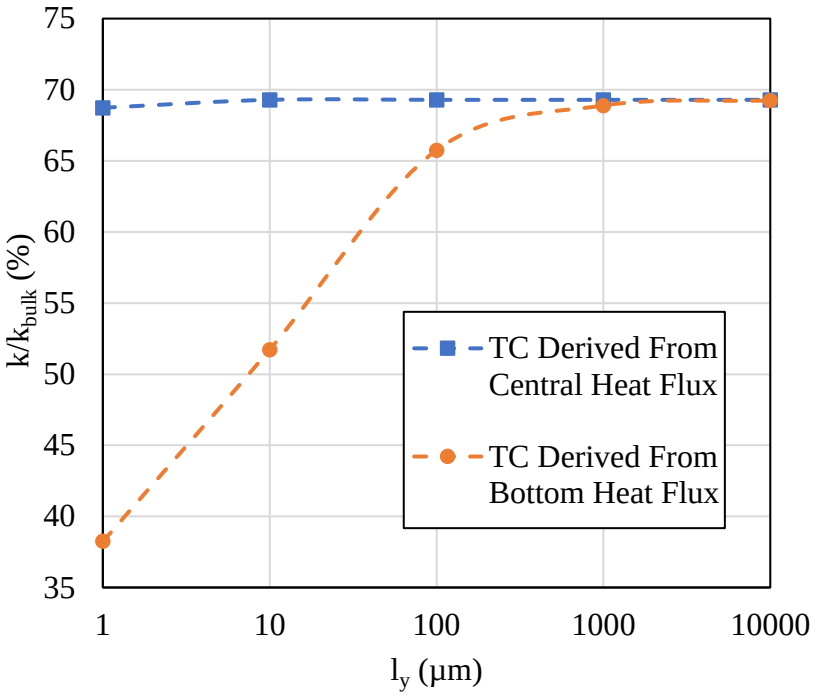


Figure 4.6. Non-dimensional thermal conductivity of 1µm Si thin film derived from central and bottom heat fluxes in terms of height.

After finding the suitable length in y-direction for the slab model the reduced thermal conductivity of thin film with any specified thickness can be calculated using Fourier law of heat conduction as

$$k_{tf} = -\vec{q}'' \frac{l_x}{\Delta T} \tag{4.2}$$

where ΔT and l_x are the initially applied temperature contrast in the x-direction and thin film thickness, respectively. Also, $\vec{q}''$ is the reduced heat flux calculated from Equation (4.1). Finally, the deduced thermal conductivity is compared with literature values. If an acceptable quantity is resulted, other thicknesses are also studied. If not, phonon properties are varied until reaching the same thermal conductivity values with the literature.

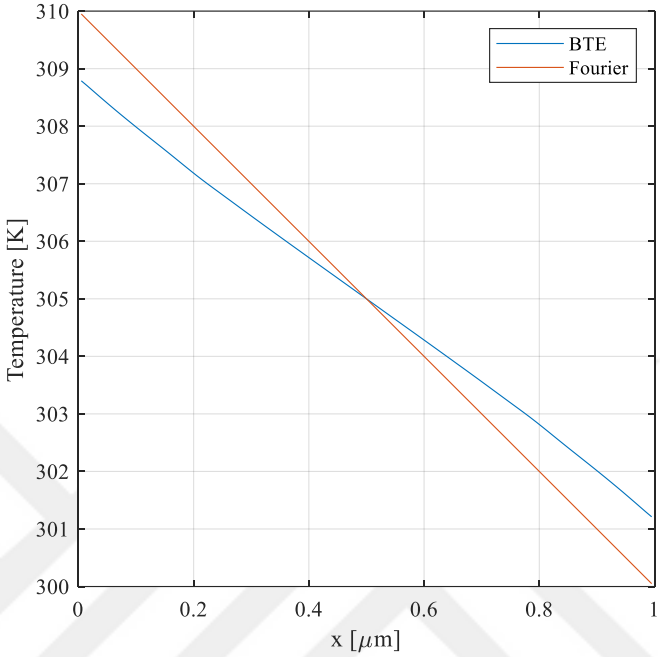


Figure 4.7. BTE and Fourier temperature profiles of the 1µm Si thin film at $y=l_y/2$.

For instance, a 1µm Si thin film is simulated applying a $\Delta T = 10\,K$ temperature difference to the boundaries while top and bottom boundaries are adiabatic. It is only important to have a temperature gradient in the x-direction for the heat to be transferred and the amount of gradient is not important. Therefore, one can apply a contrast as small as 0.1 K or as high as 100 K. Fourier temperature distribution is shown in Figure 4.3. After a number of trials, assigning 300 nm mean free path for Si as a guess, group velocity and relaxation time of Si phonons can be calculated through the kinetic theory (Equation (3.4)) being 907.4 m/s and 0.33 ns, respectively. To implement kinetic theory for these calculations, rather than using heat capacity in its mass form, isochoric form must be used which is in units of joule per kelvin per cubic meters. For this purpose, specific heats (C), are divided by material densities (ρ_d) to obtain isochoric forms (C_v) all provided in Table 1. After that Equation (3.11) is solved and BTE temperature distribution is obtained using assigned phonon properties as shown in Figure 4.4. Finally, temperature profiles are plotted for both solutions at $y=l_y/2$. It is understood from Figure 4.7 that Fourier and BTE profiles are not identical due to thermal size effects. Fourier heat flux is calculated to be $1.48 \times 10^9\, W/m^2$ while the reduced heat flux

calculated via Equation (4.1), drops down to $1.02 \times 10^9\, W/m^2$. Then the thin film thermal conductivity for a thickness of t_f is calculated through Equation (4.2) which reduces to 102 $W/m \cdot K$ where the bulk value is 148 $W/m \cdot K$. Using the same phonon properties, different thicknesses are examined and the thickness dependent nondimensional thermal conductivity is derived as shown in Figure 4.8.

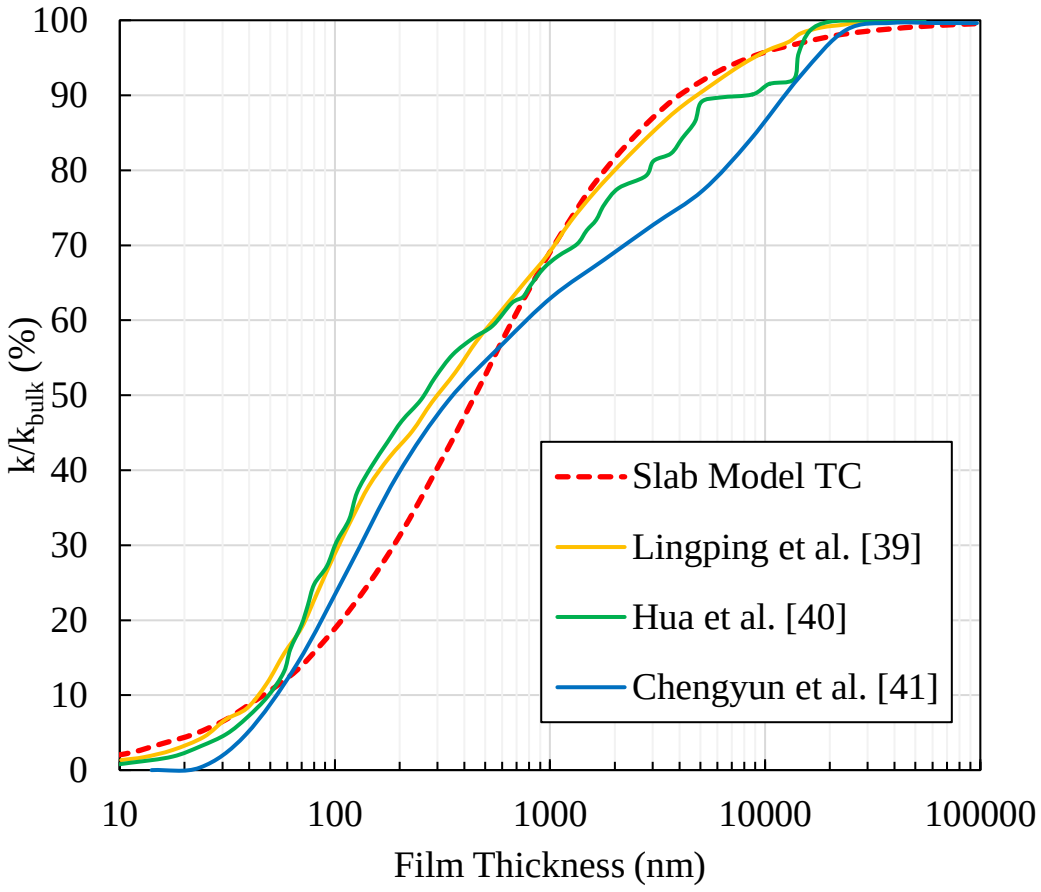


Figure 4.8. Thickness dependent thermal conductivity of Si derived from the slab model validated by results of Lingping *et al.* [39], Hua *et al.* [40], and Chengyun *et al.* [41].

In the same way, nondimensional thin film thermal conductivity spectrums are derived using validated phonon properties provided in Table 4.1. This method is used to derive thickness dependent thermal conductivities for other candidate materials with different phonon mean free paths.

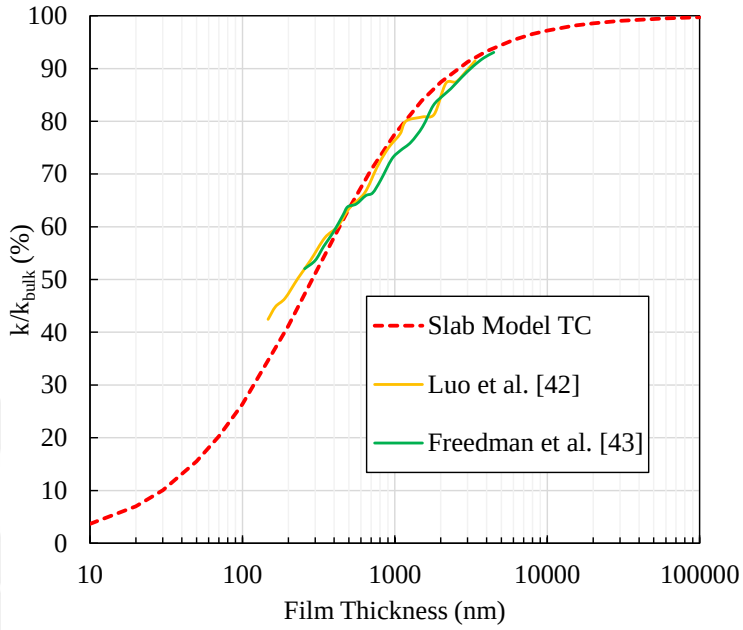


Figure 4.9. Thickness dependent thermal conductivity of GaAs derived from the slab model validated by results of Luo *et al.* [42] and Freedman *et al.* [43].

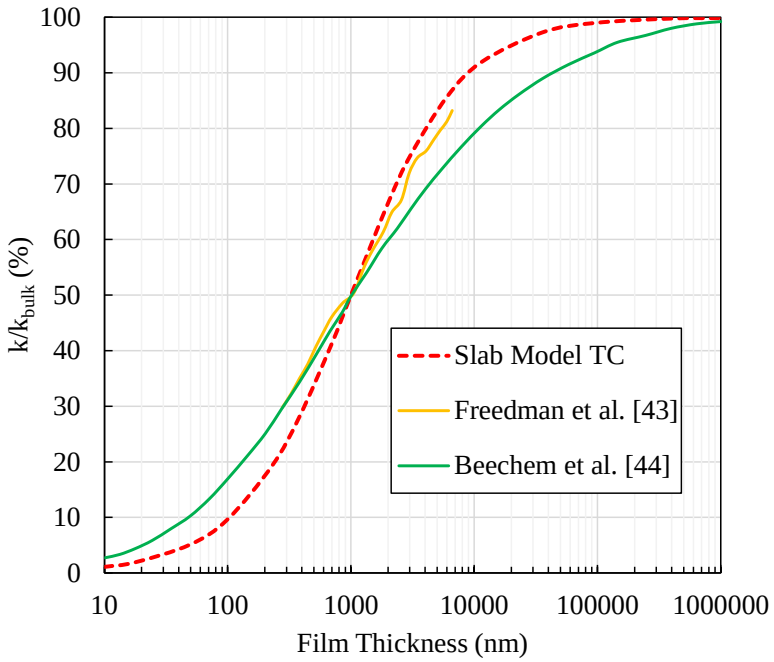


Figure 4.10. Thickness dependent thermal conductivity of GaN derived from the slab model validated by results Freedman *et al.* [43] and Beechem *et al.* [44].

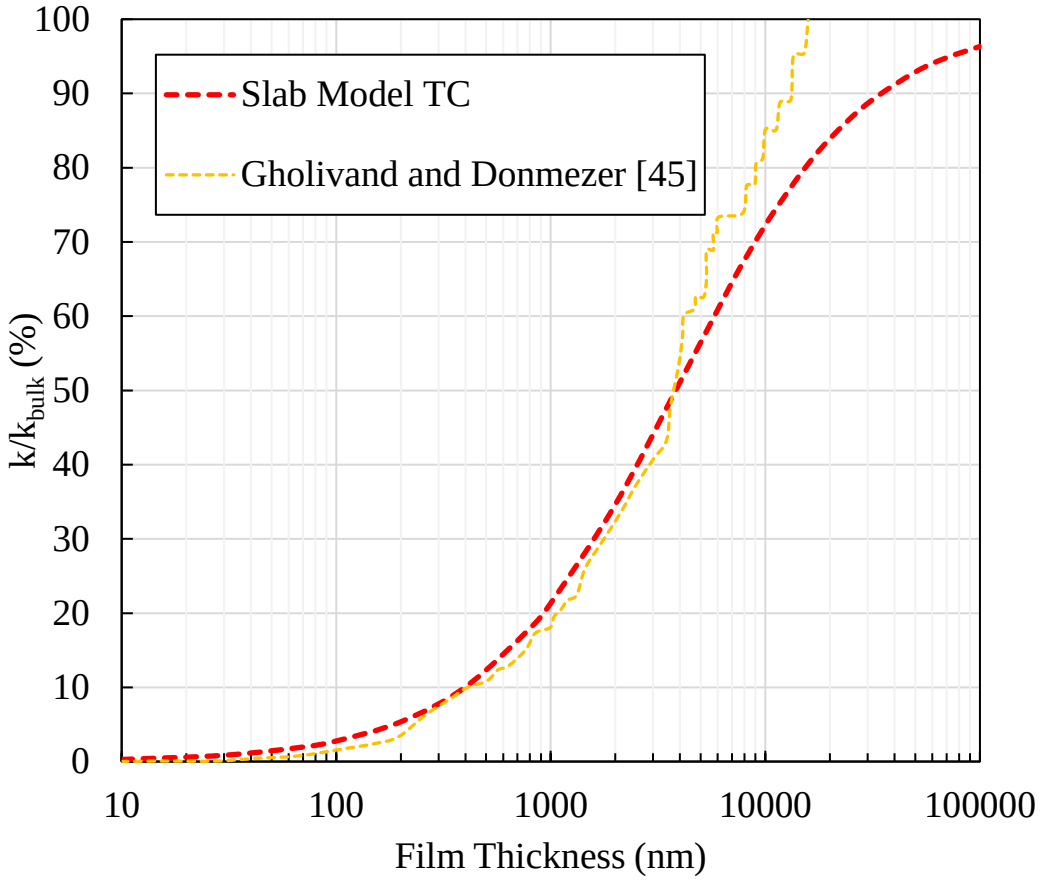


Figure 4.11. Thickness dependent thermal conductivity of MLG derived from the slab model validated by results of Gholivand and Donmezer [45].

After finding the best phonon properties matching the resulted thermal conductivity to the literature, thickness dependent values are recorded as shown in Figures 4.8 to 4.11. These properties are the main input values for the BTE solver. Therefore, using the simple slab model the correct inputs for the BTE model are derived, but also TC spectrums are derived which will be used to analyze the virtual Raman experiment model in next section.

Table 4.1. Thermal and phonon properties of GaAs, Si, GaN, and MLG materials.

Material / Property	GaAs	Si	GaN	MLG
$k\ (W/m \cdot K)$	46 [46]	148 [47]	260 [48]	3000 [49]
C (J/Kg·K)	330 [50]	700 [51]	478 [52]	100 [53]
ρ_d (Kg/m^3)	5316	2330	6150	2260
$C_v(J/m^3 \cdot K)$	1754280	1631000	2939700	226000
$\overrightarrow{v_g}$ (m/s)	403.4	907.4	390.2	15316.5
τ (ns)	0.48	0.33	1.74	0.17
Λ (nm)	195	300	680	2600

To understand the amount of size effects present in different materials, it is important to know the mean free path value of dominant heat carriers inside it. According to the Knudsen number defined as the ratio of mean free path to the characteristic length, a problem with a higher Knudsen number, deals with more size effects. For example, the temperature profiles for a 1μm thick sample for different materials are plotted in Figure 4.12. As shown in this figure, materials with higher MFP values undergo size effects in larger amounts. That is why the profile of GaN stays more distant from the Fourier profile than the profile of GaAs which has a shorter MFP. It Is worth mentioning that for any material with any bulk thermal conductivity, the Fourier temperature profile is the same.

Additionally, the derived thickness-dependent thermal conductivity of GaAs, Si, GaN, an MLG are given in Figure 4.12.

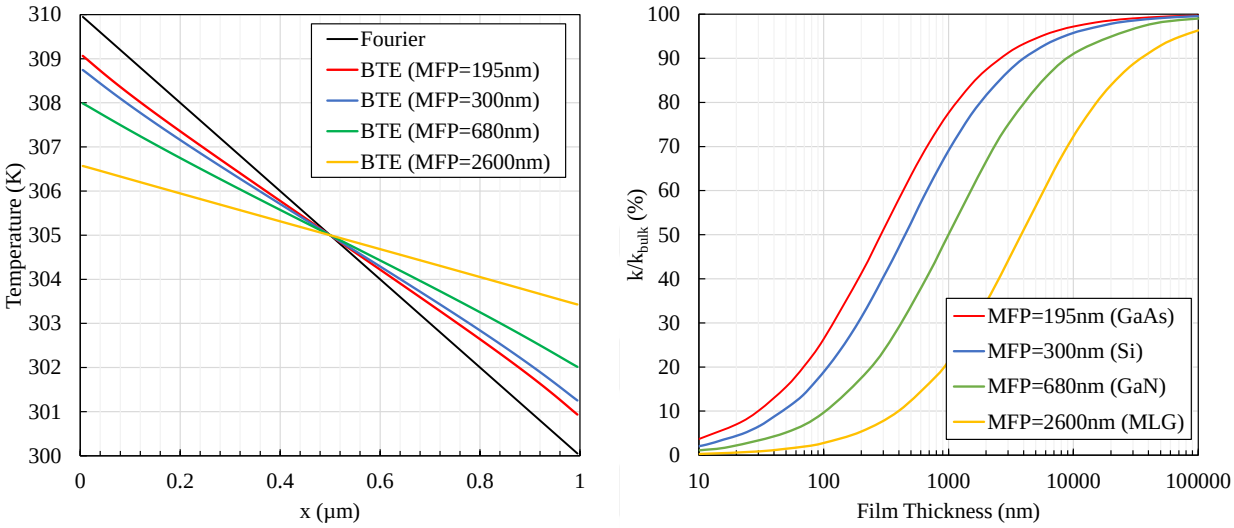


Figure 4.12. (left) BTE and Fourier temperature profiles of 1μm sample of GaAs, Si, GaN, and MLG and (right) derived thickness-dependent thermal conductivities.

4.2. Model of the Experiment (Virtual Experiment)

In this section a virtual Raman-based thermal conductivity measurement technique is developed. As stated in section 1.4, Raman spectroscopy method includes an experiment part as well as an analytical part. In a word, thermal properties for the analytical part giving the best fit to the experimental results are said to be measured values. Here, a phonon BTE solver is employed to represent the conditions during the experiment and to include thermal size effects due to ballistic-diffusive heat transport. It is worth mentioning that although our phonon BTE represents the real temperature distribution in a more accurate way than the Fourier based solutions, it does not cover the temperature variation due to mechanical stresses generated inside the specimen as a result of temperature rise in the Raman experiment. The mechanical stresses during the Raman measurements affect the Raman spectra and therefore detected temperature. As shown in the workflow in Figure 4.1, the input phonon properties for the virtual experiment are derived from the slab model.

On the other hand, the same problem is solved with a Fourier-based solve. Then the input thin film thermal conductivity is differed for each thickness to match the Fourier maximum temperature to the BTE maximum temperature. The one giving the best maximum temperature prediction is deduced as the thin film thermal conductivity of thin film.

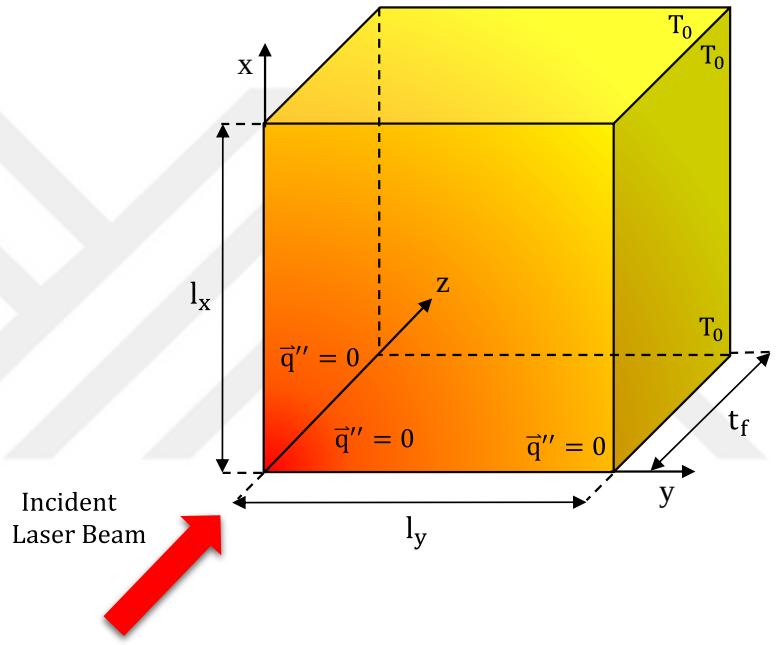


Figure 4.13. Schematic of the 3D virtual Raman experiment model with applied boundary conditions and model parameters.

To simulate the Micro-Raman experiment real conditions, a volumetric heat generation is added to the initial Fourier and phonon BTE solvers. This heat generation is appeared as q''' in Equations (3.11) and (3.12). This term is a function of position (x, y, and z) which includes laser beam properties as well as material of interest's optical properties. When an incident light is shined onto a surface of a thin film, a portion of this is reflected and the other portion is absorbed by the sample. Assuming that all the absorbed energy from the incident light is converted into heat generation inside the specimen, the intensity of light that is not reflected ($I_{non-refl.}$) is calculated by

$$I_{non-refl.} = (1 - \rho)\, I_0 \tag{4.3}$$

where ρ is the reflectance of the material at the probing wavelength (λ) of laser beam and I_0 is the intensity of incident light [54]. The probing wavelength is assumed to be 532nm in all our simulations.

After subtracting the reflected amount of incident light, according to Beer-Lambert's law the remaining intensity is absorbed through the thickness of the sample as given in

$$I(z) = I_{non-refl.} e^{-\alpha z} \tag{4.4}$$

which is a function of depth (distance from z-axis origin) and absorption coefficient α.

The rate of volumetric heat generation is

$$q'''(z) = \alpha I(z) = \alpha(1 - \rho) e^{-\alpha z} I_0 \tag{4.5}$$

which is proportional to absorbed intensity $I(z)$ where the proportionality constant is the absorption coefficient α, that is also a material-dependent optical property at the probing wavelength. Therefore, z-dependent heat generation rate is calculated by Equation (4.5). This function presents a relation between the intensity of incident light and volumetric heat generation as a function of depth. To correctly model the Gaussian laser beam profile, TEM_{00} mode [55] is used in equation

$$I_0 = \frac{2P}{\pi \omega(z)^2} e^{\frac{-2r^2}{\omega(z)^2}} \tag{4.6}$$

to modify the intensity of the incident light in order for it to be a fuction of total laser operating power P, radial distance r, and $\omega(z)$ which is the radius of the laser beam at distance z that the intensity drops down to $1/e^2 \approx 13.53\%$.

Finally, by changing the radial distance r to $\sqrt{x^2 + y^2}$, the volumetric heat source for our simulations can be written as

$$q'''(x,y,z) = (1-\rho)\alpha e^{-\alpha z}\frac{2P}{\pi\omega(z)^2}e^{\frac{-2(x^2+y^2)}{\omega(z)^2}} \tag{4.7}$$

where $\omega(z)$ can be found from equation

$$\omega(z) = \omega_0\sqrt{1+\frac{z^2}{z_R^2}} \tag{4.8}$$

which includes laser beam waist radius ω_0, and the Rayleigh range z_R. The waist radius is considered to be 362 nm in all the simulations.

Furthermore, the Rayleigh range is calculated by

$$z_R = \frac{\pi\omega_0^2 n}{\lambda} \tag{4.9}$$

which is a function of material refractive index n at the excitation wavelength of the Raman laser beam λ.

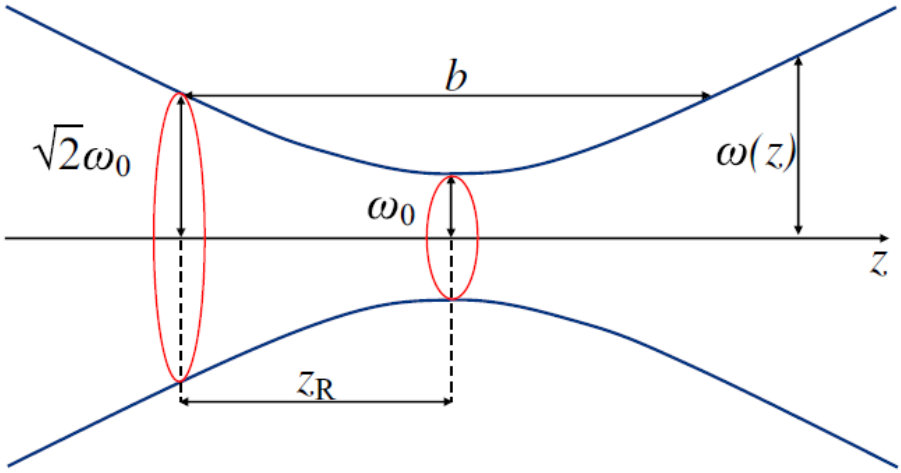


Figure 4.14. Gaussian laser beam where ω_0, z_R and $\omega(z)$ are waist radius, Rayleigh range and laser beam radius at distance z Reprinted by permission from Elsevier [56]. License number: 5237030873237.

Laser beam radius in the focal plane ($z = 0$) is considered to be equal to ω_0 where the light intensity reaches its maximum and decays by propagating in the z-direction and spreads a small amount in the radial direction as shown in Figure 4.14.

Table 4.2. Optical properties of materials at the probing wavelength of 532nm and room temperature (300 K).

Material / Property	GaAs	Si	GaN	MLG
α (cm^{-1})	70154 [57]	12233 [58]	16527 [59]	5836.8 [60]
ρ	0.37446 [57]	0.37437 [58]	0.16111 [59]	0.19179 [60]
n	4.0668 [61]	4.1432 [62]	2.4236 [63]	2.6793 [64]

4.2.1. Grid Study

To find the optimal grid size for 3D simulations, a mesh study is performed. For this purpose, a standard 1μm×1μm×1μm Silicon model is developed as shown in Figure 4.13. A Raman beam with a power of 10 mW, probing wavelength of 532 nm, and waist radius of 362 nm is shined onto the model. The localized heating process starts from the surface that is exposed to the Raman laser that is the x-y plane in z=0. Gradient of the most important variable that is temperature, occurs at x=y=z=0 position. In other words, the maximum temperature reached in the numerical simulation that will be used for thermal conductivity determination, is the most important result of the study. Therefore, the highest temperature is chosen as the case of grid study. At each step the number of rectangular meshes are increased

and maximum temperature is recorded. Figure 4.15 shows the maximum temperature variation versus the number of elements along any edge of the model.

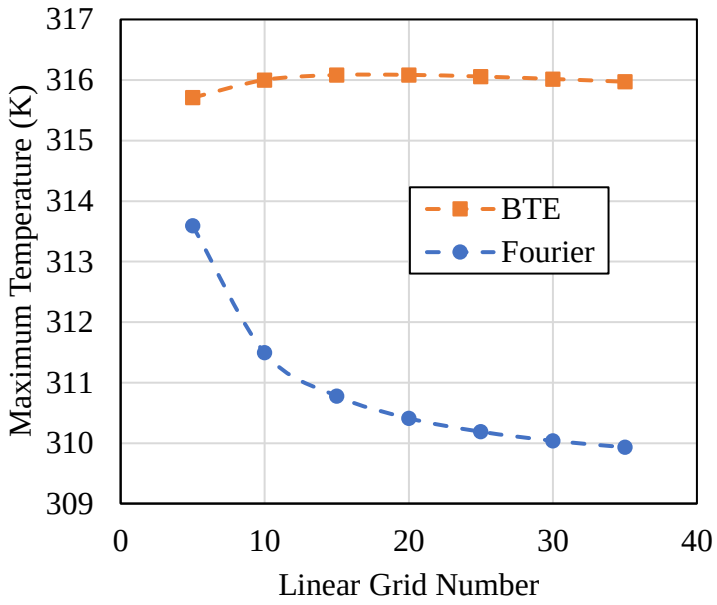


Figure 4.15. Grid independence study for the 3D model.

The difference between the Fourier maximum temperature of 25×25×25 and 20×20×20 drops down to 0.07% where the BTE maximum temperature stays almost the same. Therefore, the 20×20×20 system is considered to be sufficient for a 1µm×1µm×1µm domain for the results not to depend on grid structure. Since the geometry will be changed in our simulations for different thicknesses, the suitable mesh sizes are chosen in a way that an element's size does not exceed 50 nm. For example, in a 2µm×2µm×2µm domain, for elemental rectangular control volume not to exceed 50 nm, a 40×40×40 grid system must be developed.

4.2.2. Domain Size Study (Boundary effects)

Additional to grid independency study, a domain size independency examination is performed. As shown in the problem schematic in Figure 4.13, three sides are given kept at constant temperatures (T_0 = 300 K) and they affect the maximum temperature values reached during the virtual experiment. Therefore, they should be kept as distant as they do not affect

maximum temperature. For this purpose, a 1 µm thin film is exposed to a Raman laser beam the same as the one in the grid study section. However, this time the length of the model in x and y directions is increased in the same boundary conditions as well as the same heat generation. At each step, the most critical variable, maximum temperature is recorded as shown in Figure 4.16. Changes in the maximum temperature is plotted versus the ratio of length to thickness. The difference between the maximum temperature drops below 0.1% from l_x/l_y=2 to l_x/l_y=2.5 as shown in Figure 4.16.

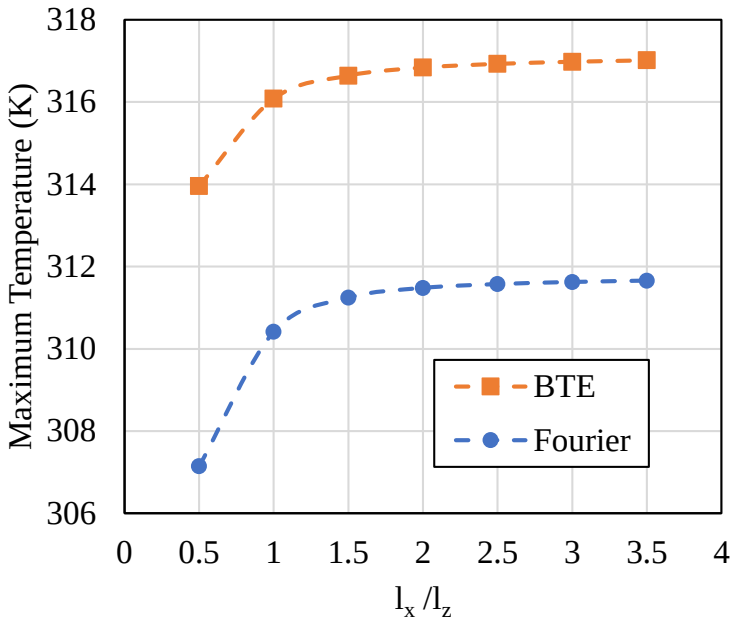


Figure 4.16. Length independency study for temperature measurement.

Therefore, it is required for l_x to be at least two times the thickness of the film to be able to neglect boundary effects on temperature measurement which means if we use two symmetry conditions in x and y directions, the length of the specimen should be at least four times its thickness. In fact, sub-micron thin film specimens in real life are provided in relatively higher ratios but simulating the whole sample requires high computational time and cost and is not efficient.

4.2.3. Results

After finding the suitable mesh structure, the problem dimensions are defined according to section 4.2.2. Then the temperature distribution is derived using both BTE and Fourier solutions. Figure 4.17 shows the 3D temperature distribution of Fourier and BTE solution of 1µm Si thin film under a laser power of 10mW and 532 nm probing wavelength with a waist radius of 362 nm.

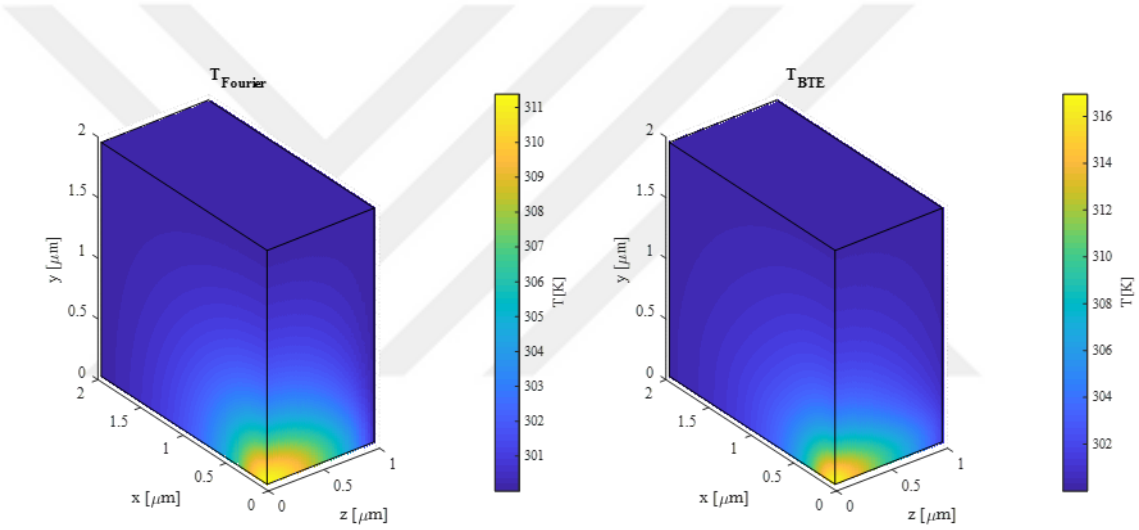


Figure 4.17. 3D temperature distribution of (left) Fourier and (right) BTE solutions for a 1µm Si thin film.

The temperature distribution on the most critical faces for the Fourier and BTE solutions are also shown in Figure 4.18 and 4.19.

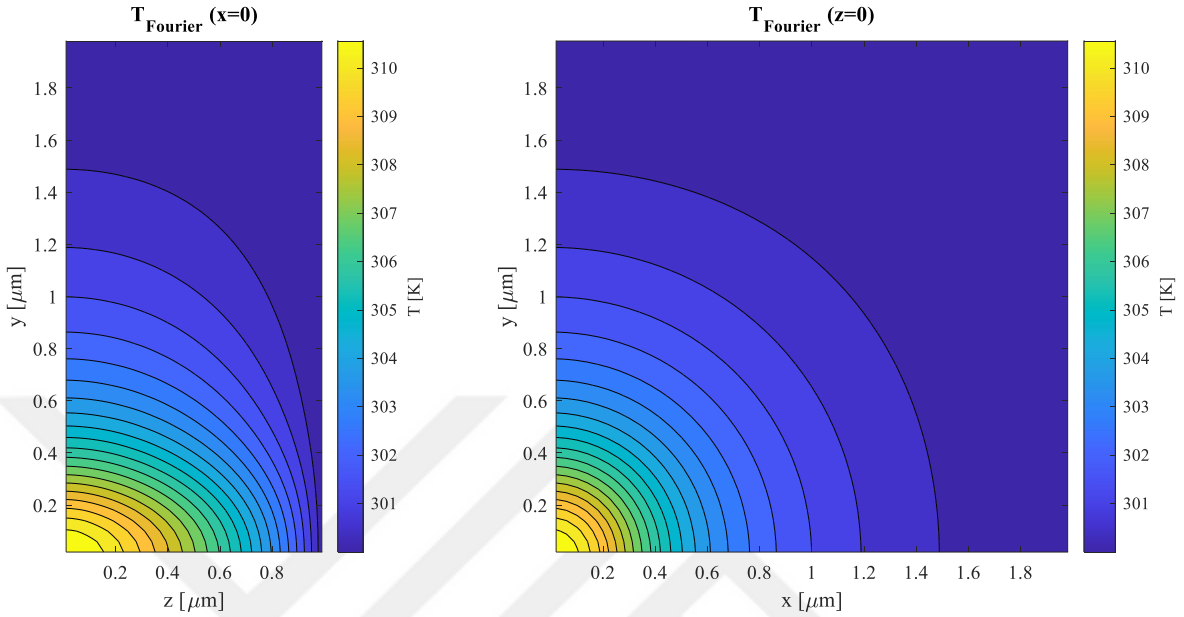


Figure 4.18. Temperature contour of the Fourier solution on the (left) z-y and (right) x-y plane.

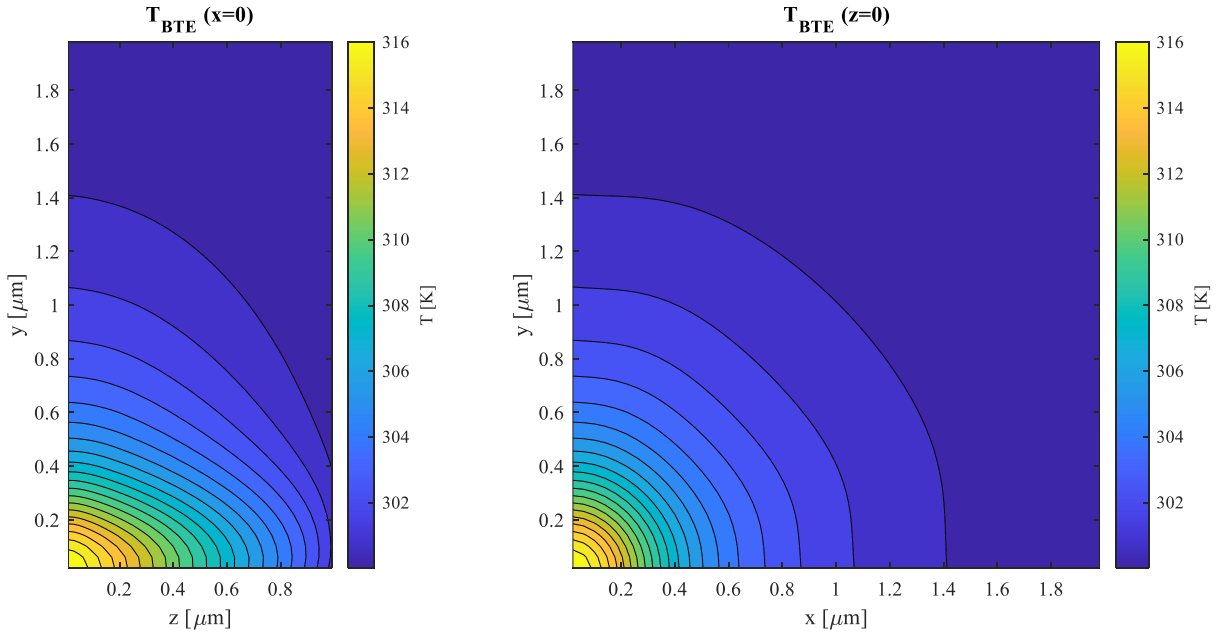


Figure 4.19. Temperature contour of the BTE solution on the (left) z-y and (right) x-y plane.

Furthermore, temperature profiles along the x and z axis are plotted in Figure 4.20. As shown in this figure maximum temperature occurs right in the center of the sample on the face exposed to the laser beam.

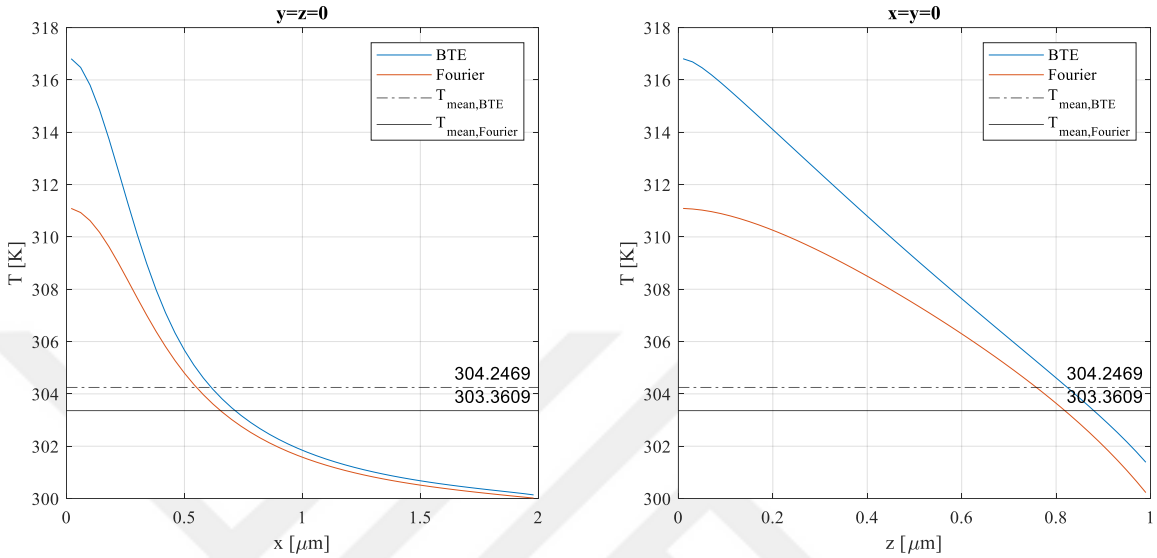


Figure 4.20. BTE and Fourier temperature profiles along the (left) radial (x or y) and (right) axial (z) directions of 1μm Si thin film with 10mW laser power.

In the conventional Raman thermometry, the local temperature is measured during the experiment which is in fact an average of temperature inside the probing region. Because of the localized heating, an infinitesimal region is heated up in which the temperature should be detected. Therefore, the smaller the averaging region, the more accurate temperature measurement. Mean temperature values shown in Figure 4.20 represent an average temperature in a cubic region with a length of waist radius and depth of $1/\alpha$ which is considered to be the penetration depth for each material. However, to match the Fourier results with the BTE results to find thin film thermal conductivity, the maximum temperature values are examined in next chapter which is more accurate than the average temperature approach.

Finally, to understand thermal size effects due to ballistic-diffusive heat transport during the Raman experiment, the difference between the maximum BTE temperature and maximum Fourier temperature is recorded. To have a better insight, the data is extracted for each material, at two different thicknesses 100 nm and 200 nm and three different laser operating powers 10 mW, 50 mW, and 100 mW. Figures 4.21 to 4.24 show the results for Si, GaN, GaAs, and MLG, respectively.

For the laser power of 10 mW in the 100 nm Si thin film there is a 3.8 K difference between maximum temperatures while it increases to 5.3 K for the 200 nm thin film in the same power. The initial maximum difference 3.8 K increases to 19.2 K and 38.4 K for 50 mW and 100 mW powers, respectively. It is deduced from Figure 4.21 that the slope of 200 nm thin film is sharper than the 100 nm one.

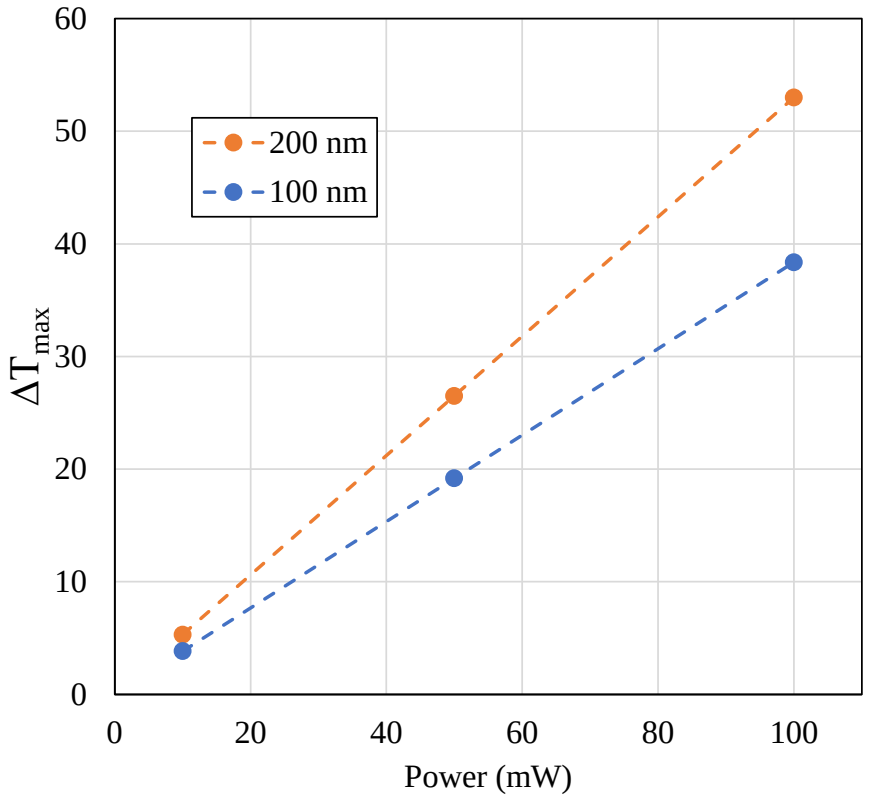


Figure 4.21. Variation of maximum temperature difference between BTE and Fourier for 100 nm and 500 nm Si thin films for laser powers of 10 mW, 50 mW, and 100 mW in the same probing wavelength of 532 nm and waist radius of 362 nm.

For the laser power of 10 mW in the 100 nm GaN thin film there is a 9.2 K difference between maximum temperatures while it increases to 13.1 K for the 200 nm thin film in the same power. The initial maximum difference 9.2 K increases to 45.8 K and 91.6 K for 50 mW and 100 mW powers, respectively. It is also deduced from Figure 4.22 that the slope of 200 nm thin film is sharper than the 100 nm one.

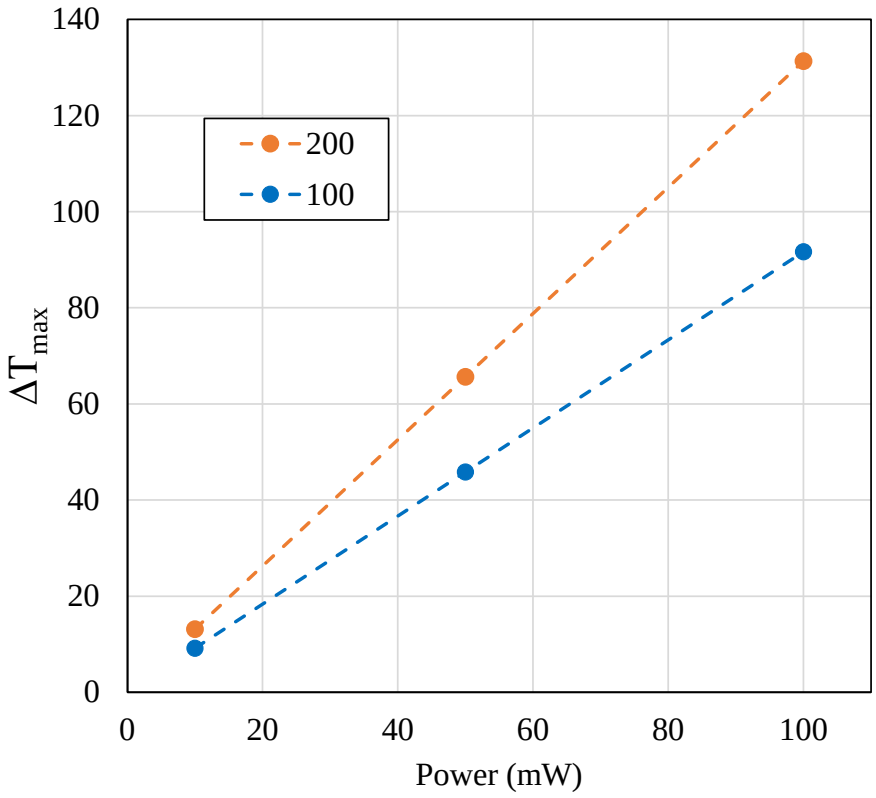


Figure 4.22. Variation of maximum temperature difference between BTE and Fourier for 100 nm and 500 nm GaN thin films for laser powers of 10 mW, 50 mW, and 100 mW in the same probing wavelength of 532 nm and waist radius of 362 nm.

For the laser power of 10 mW in the 100 nm GaAs thin film there is a 35.1 K difference between maximum temperatures while it increases to 38.1 K for the 200 nm thin film in the same power. The initial maximum difference 35.1 K increases to 175.6 K and 351.2 K for 50 mW and 100 mW powers, respectively. It is deduced from Figure 4.23 that the slope of 200 nm thin film is sharper than the 100 nm one.

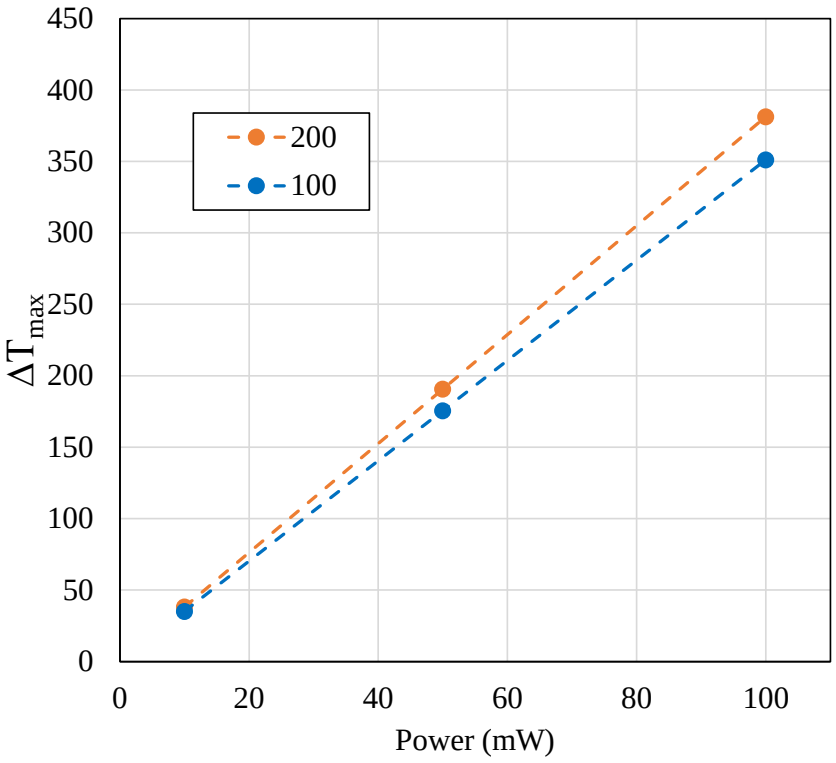


Figure 4.23. Variation of maximum temperature difference between BTE and Fourier for 100 nm and 500 nm GaAs thin films for laser powers of 10 mW, 50 mW, and 100 mW in the same probing wavelength of 532 nm and waist radius of 362 nm.

For the laser power of 10 mW in the 100 nm MLG thin film there is a 1.1 K difference between maximum temperatures while it increases to 1.67 K for the 200 nm thin film in the same power. The initial maximum difference 1.1 K increases to 5.5 K and 11 K for 50 mW and 100 mW powers, respectively. It is deduced from Figure 4.24 that the slope of 200 nm thin film is sharper than the 100 nm one.

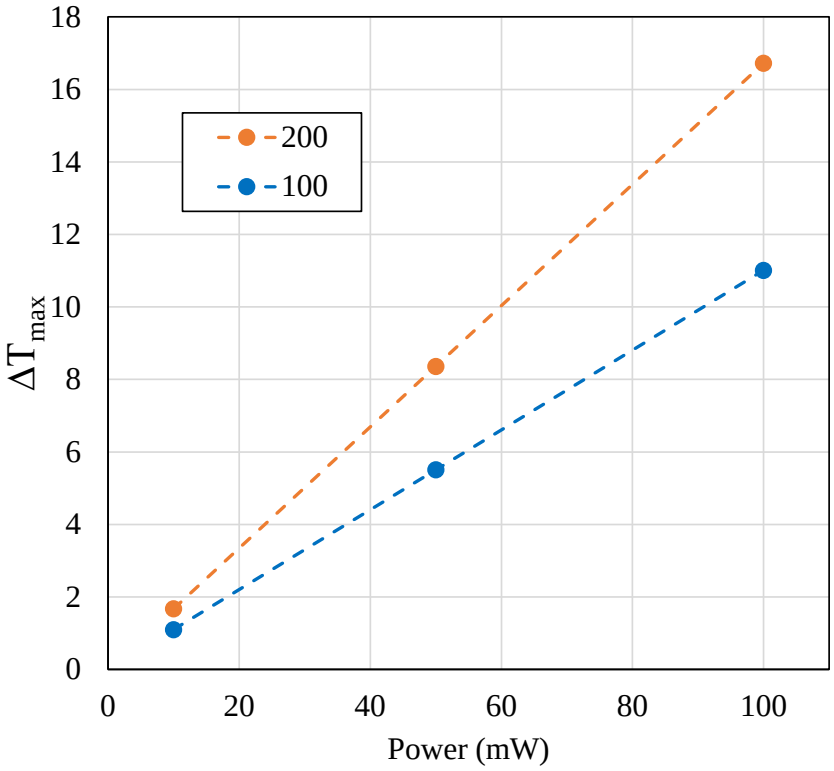


Figure 4.24. Variation of maximum temperature difference between BTE and Fourier for 100 nm and 500 nm MLG thin films for laser powers of 10 mW, 50 mW, and 100 mW in the same probing wavelength of 532 nm and waist radius of 362 nm.

4.3. Conclusions

- Thickness dependent thermal conductivities derived by the simple slab model are in a good agreement with the literature.

- As shown in Figure 4.12, boundary scattering effects become more dominant for materials with longer mean free path. For example, the slab model temperature profile of GaN becomes more distracted from Fourier than the profile of Si since it has a higher mean free path value.

- According to the findings from the slab model, the thickness dependency of thermal conductivity of any material is a function of phonon mean free path.

- With the help of model of virtual Raman experiment, thermal behavior of the specimen during the real experiment conditions can be predicted more accurately by using the phonon BTE solution rather than Fourier.

- The difference between BTE and Fourier maximum temperatures, increase by increasing the laser power as well as increasing the film thickness.

- GaAs is the most sensitive material amongst the others. Therefore, lower laser powers must be used to prevent degradation of the specimen due to high temperatures.

- For its comparatively high thermal conductivity and phonon mean free path, MLG is the least sensitive material to the laser power. Therefore, to observe a detectable temperature rise, a relatively higher laser power should be used in its Raman measurements.

5. ERROR ANALYSIS OF CONVENSIONAL COMPLEMENTARY MODEL

To find the reduced thin film thermal conductivity using the virtual Raman experiment developed in this study, first the maximum BTE temperature is deduced. Then the same problem is simulated with a Fourier solver as shown in Figure 5.1 and its maximum temperature is derived as well. Then the input thermal conductivity to the Fourier solver is reduced until obtaining the same maximum temperature as the BE solution. One thermal conductivity giving the best match to maximum temperatures are recorded as the thin film thermal conductivity by the old technique (k_{tf}^*). To evaluate the results deduced from the virtual Raman experiment developed for this study, the error between thermal conductivity derived from this method and slab model derived thermal conductivity is calculated by equation

$$Error\ (\%) = \frac{k_{tf} - k_{tf}^*}{k_{tf}} \times 100 \tag{5.1}$$

where k_{tf} and k_{tf}^* are thermal conductivities derived from slab model and virtual Raman experiments, respectively.

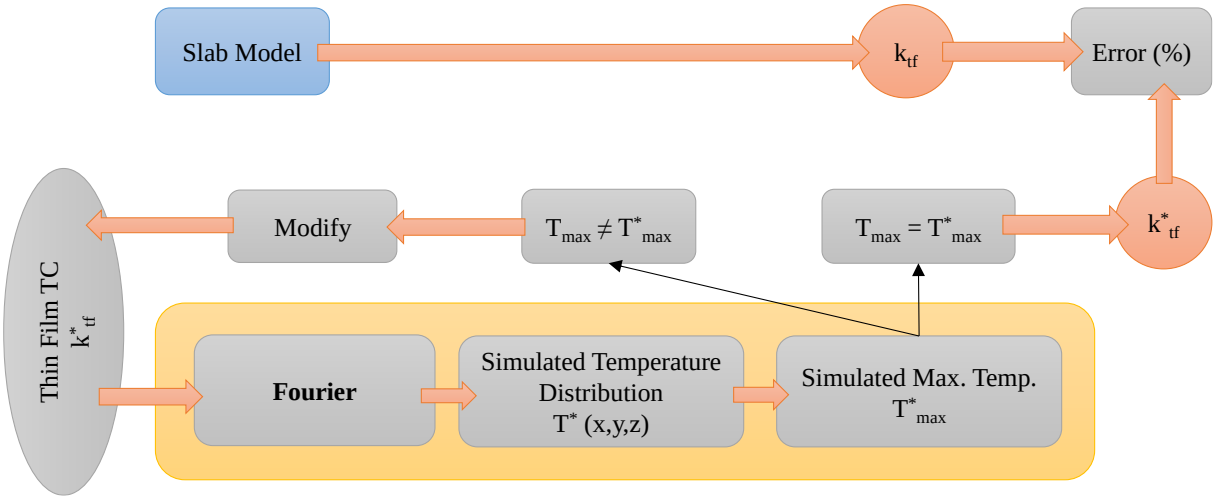


Figure 5.1. The workflow of finding thin film thermal conductivity by the virtual Raman experiment and its error using the slab model.

Table 5.1 includes thermal conductivities of the studied materials derived from the slab model for two different thicknesses (100 nm and 500 nm). This table includes derived maximum Fourier and BTE temperatures with the bulk thermal conductivities as an input. Then the input thermal conductivity for the Fourier solver is reduced down to one represented in Table 5.1 to obtain the maximum temperature deduced from the BTE solver.

Figures 5.2, 5.3, 5.4, and 5.5 show the calculated thermal conductivities through the virtual Raman experiment compared with the results from the slab model for GaAs, Si, GaN, and MLG materials, respectively.

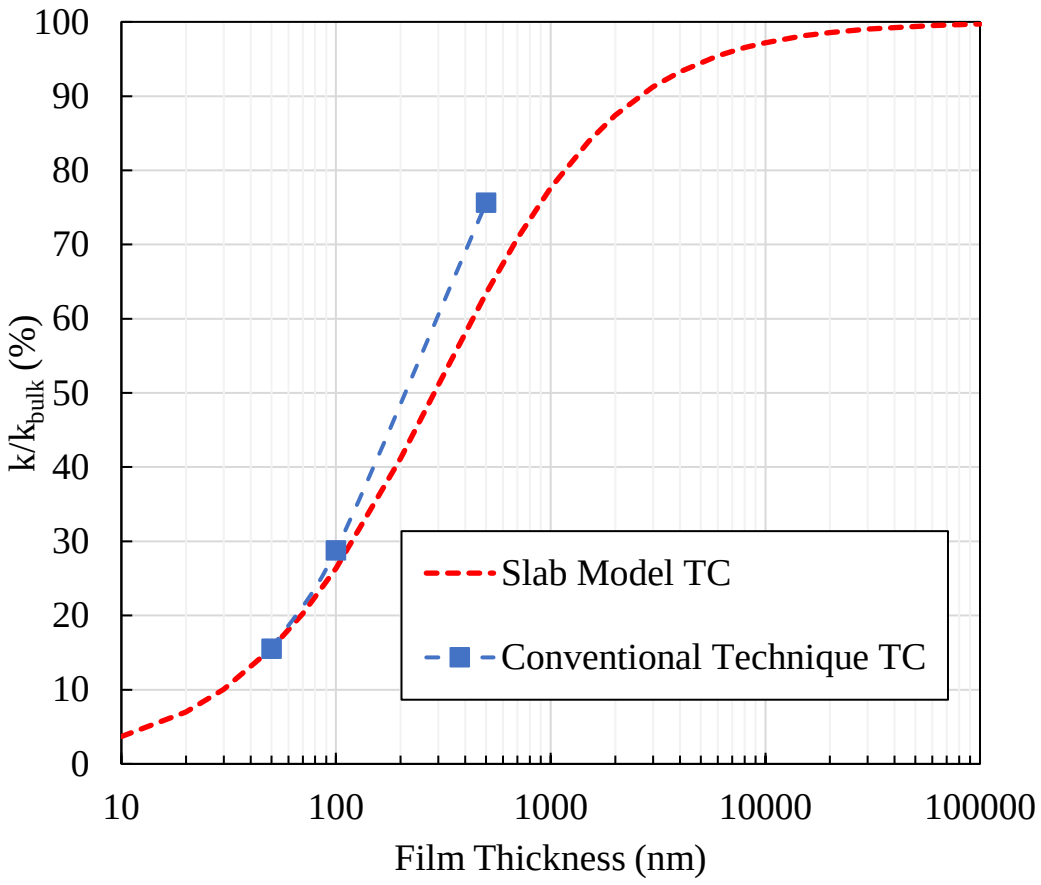


Figure 5.2. Nondimensional thermal conductivity of GaAs compared to the results of the slab model.

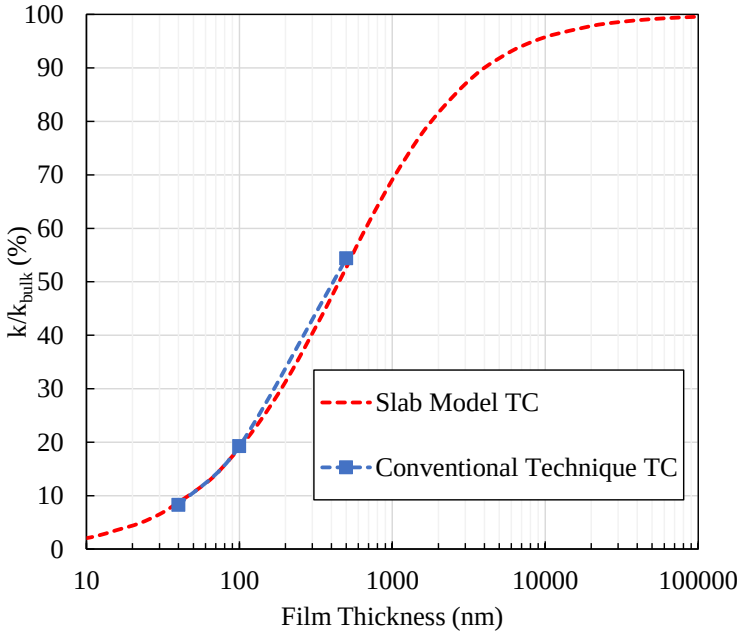


Figure 5.3. Nondimensional thermal conductivity of Si compared to the results of the slab model.

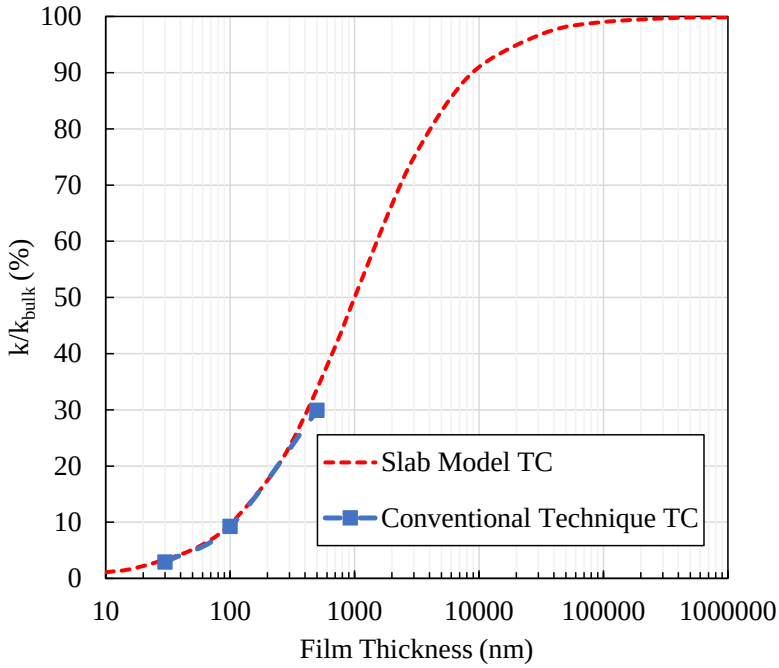


Figure 5.4. Nondimensional thermal conductivity of GaN compared to the results of the slab model.

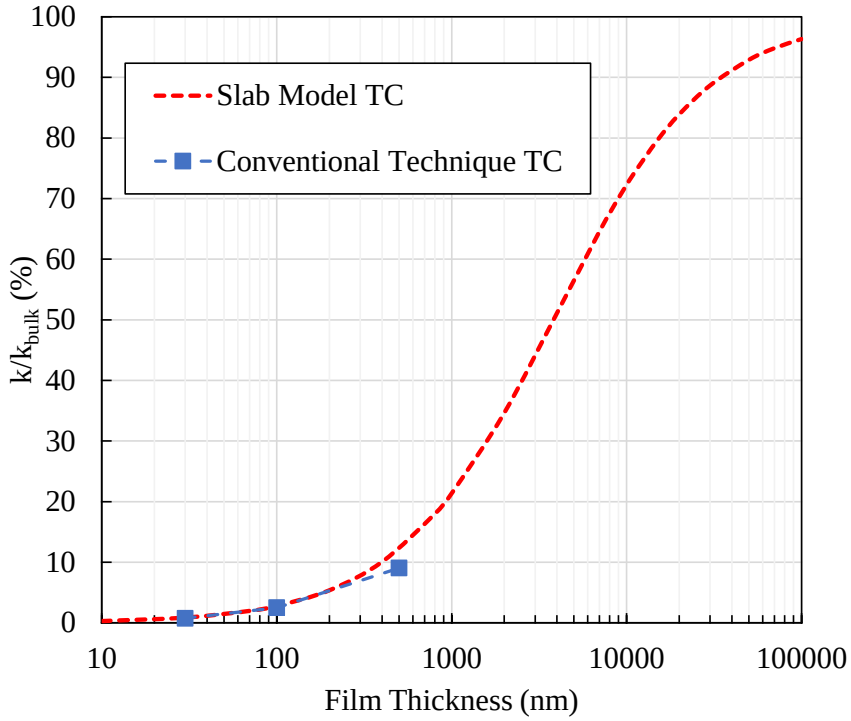


Figure 5.5. Nondimensional thermal conductivity of MLG compared to the results of the slab model.

Table 5.1. Error analysis of virtual Raman-based thermal conductivity measurement.

	GaAs	Si	GaN	MLG	Thickness (nm)
k_{tf}/ k_{bulk} (%)	26.37	19.12	9.66	2.78	100
	63.45	53.07	33.66	12.20	500
$T_{max, Fourier}$ (k_{bulk})	314.2005	300.9114	300.9273	300.0283	100
	376.6387	307.1067	306.9516	300.2338	500

Table 5.1. Error analysis of virtual Raman-based thermal conductivity measurement (cont.).

$T_{max,\ BTE}$ (k_{bulk})	349.3204	304.7476	310.0902	301.1294	100
	401.0361	313.0543	323.2555	302.5891	500
k_{tf}^{*}/ k_{bulk} (%)	28.80	19.26	9.23	2.5	100
	75.65	54.39	29.88	9.03	500
$T_{max,\ Fourier}$ (k_{tf})	349.2998	304.7331	310.046	301.1306	100
	401.596	313.0657	323.2616	302.5886	500
Error (%)	-9.22	-0.73	4.45	10.07	100
	-19.23	-2.49	11.23	25.98	500

5.1. Conclusions

- The old Raman thermometry technique which uses a Fourier based complementary method may overestimate or underestimate thin film thermal conductivity of thin films according to the errors calculated in Table 5.1.

- The performance of virtual Raman experiment to measure thin film thermal conductivity is better for relatively lower thicknesses.

- For a specific thin film thickness, measured thermal conductivity for a material with a higher mean free path is associated with a higher error due to dominant thermal size effects.

6. CONCLUSIONS AND FUTURE WORK DIRECTIONS

6.1. Conclusions

Because of their wide range of application in microelectronic devices, thin films need to be thermally characterized for device thermal management purposes. Theoretical techniques suffer from their high computational time and cost. While experimental methods setups are expensive and hard to calibrate. In this study, a numerical method is introduced as a substitution for the Raman-based thermal conductivity measurement technique. The real conditions during the actual experiment are simulated via the gray Boltzmann Transport Equation. This solver gives a better estimation of the temperature distribution by including thermal size effects originating from localized heating and boundary scattering effects. The resulted thermal conductivities are compared to the data from a simple slab model which is initially validated by the literature data. Thickness dependent thermal conductivities are derived for GaAs, Si, GaN, and MLG materials which are promising candidates in the semiconductor technology. The results show that materials like MLG that have higher phonon mean free paths, undergo larger thermal size effects which can cause erroneous calculation of their thermal conductivity as well as temperature prediction by Fourier law of heat conduction.

6.2. Future Work Directions

To improve the conventional Raman-based thermal conductivity measurement, it is suggested to use the phonon BTE instead of the Fourier based thermal model. In fact, the Fourier law of heat conduction fails to correctly predict the temperature in the presence of thermal size effects. Therefore, it gives an erroneous reduced thermal conductivity of a thin film. Accordingly, the micro-Raman based thermal characterization coupled with the BTE thermal model is more accurate than the one coupled with a Fourier model.

Figure 6.1 shows the suggested procedure for the future micro-Raman based thermal conductivity measurement. According to the modified technique, the complementary thermal model should no longer be a Fourier based one due to the size effects originating from not only the boundary confinement in thin films, but also the localized heating during the Raman experiment as addressed in the results section. In this method, phonon properties like mean free path is guessed instead of thermal conductivity itself. Using this property, the maximum temperature is estimated by the virtual Raman model developed in this study. If the measured and simulated maximum temperatures be not equal, the guessed phonon property is changed until resulting in the same maximum temperatures. Finally, after that the correct phonon properties are deduced, they are put into the simple slab model developed in this work to obtain thickness dependent thermal conductivity of any material.

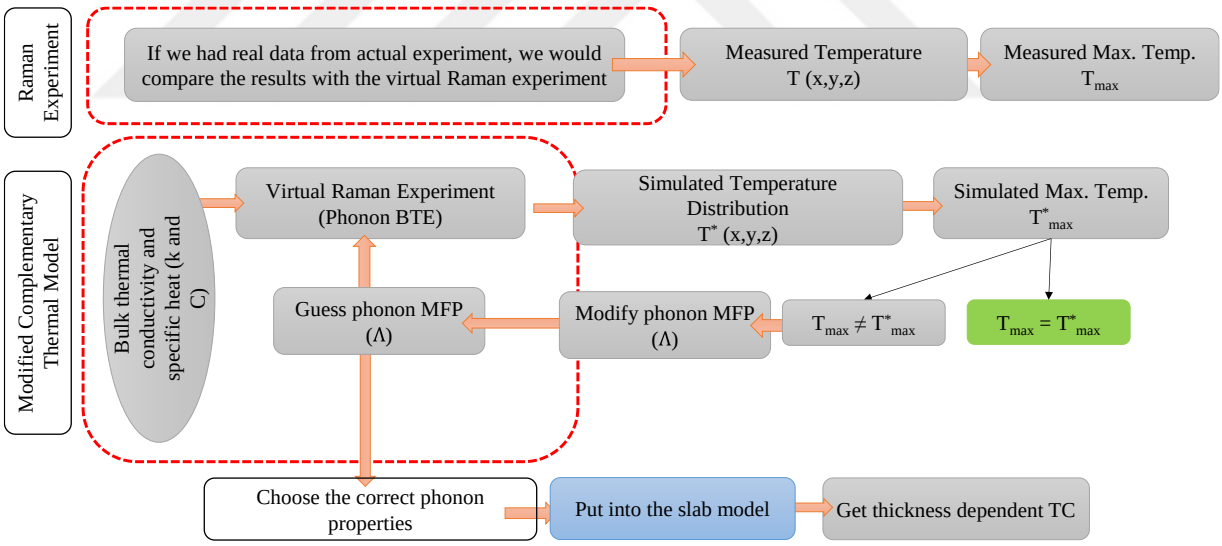


Figure 6.1. Workflow of suggested technique for future works.

REFERENCES

1. Aberle, A. G., “Fabrication and Characterisation of Crystalline Silicon Thin-Film Materials for Solar Cells”, *Thin Solid Films*, vol. 511–512, pp. 26–34, 2006.

2. Thomas, S. R., P. Pattanasattayavong, and T. D. Anthopoulos, “Solution-Processable Metal Oxide Semiconductors for Thin-Film Transistor Applications”, *Chemical Society Reviews*, vol. 42, no. 16, pp. 6910–6923, 2013.

3. Takada, N., T. Tsutsui, and S. Saito, “Control of Emission Characteristics in Organic Thin-Film Electroluminescent Diodes Using an Optical-Microcavity Structure”, *Applied Physics Letters*, vol. 63, no. 15, pp. 2032–2034, 1993.

4. Myny, K., S. Smout, M. Rockelé, A. Bhoolokam, T. H. Ke, S. Steudel, B. Cobb, A. Gulati, F. G. Rodriguez, K. Obata, M. Marinkovic, D. V. Pham, A. Hoppe, G. H. Gelinck, J. Genoe, W. Dehaene , and P. Heremans, “A Thin-Film Microprocessor with Inkjet Print-Programmable Memory”, *Scientific Reports*, vol. 4, pp. 1–6, 2014.

5. Zandi, S., M. J. Seresht, A. Khan, and N. E. Gorji, “Simulation of Heat Loss in Cu2ZnSn4SxSe4−X Thin Film Solar Cells: A Coupled Optical-Electrical-Thermal Modeling”, *Renewable Energy*, vol. 181, pp. 320–328, 2022.

6. Kuo, Y., “Thin Film Transistor Technology-Past, Present, and Future”, *The Electrochemical Society Interface*, vol. 22, no. 1, pp. 55–61, 2013.

7. Daus, A., S. Han, S. Knobelspies, G. Cantarella, and G. Tröster, “Ge2Sb2Te5 P-Type Thin-Film Transistors on Flexible Plastic Foil”, *Materials (Basel)*, vol. 11, no. 9, 2018.

8. Liu, H. Y., C. S. Lee, and Y. C. Yang, “Improved Light Output Power of InGaN/GaN LED by Using Ultrasonic Spray Pyrolysis Deposited MgO”, *IEEE Transactions on Electron Devices*, Aug. 2017, vol. 64, no. 8, pp. 3246–3251, 2017.

9. Kise, K., M. N. Fujii, S. Urakawa, H. Yamazaki, E. Kawashima, S. Tomai, K. Yano, D. Wang, M. Furuta, Y. Ishikawa, and Y. Uraoka, “Thermal Analysis of Amorphous Oxide Thin- Film Transistor Degraded by Combination of Joule Heating and Hot Carrier Effect”, *Applied Physics Letters*, vol. 053506, no. 5, 2013.

10. In, H. J. and O. K. Kwon, “External Compensation of Non-Uniform Electrical Characteristics of Thin-Film Transistors and Degradation of OLED Devices in AMOLED Displays,” *IEEE Electron Device Letters*, vol. 30, no. 4, pp. 377-379, 2009.

11. Chatterjee, B., C. Dundar, T. E. Beechem, E. Heller, D. Kendig, H. Kim, N. Donmezer, and S. Choi., “Nanoscale Electro-Thermal Interactions in AlGaN / GaN High Electron Mobility Transistors”, *Journal of Applied Physics*, vol. 127, no. 4, p. 044502, 2020.

12. Christenson, J. G., M. P. Kroonblawd, R. A. Austin, L. E. Fried, and R. J. Phillips, “Simulating Transient Heat Transfer in Graphene at Finite Knudsen Number via The Boltzmann Transport Equation and Molecular Dynamics”, *Physical Review B*, vol. 102, no. 20, p. 205406, 2020.

13. Regner, K. T., D. P. Sellan, Z. Su, C. H. Amon, A. J. H. Mcgaughey, and J. A. Malen, “Broadband Phonon Mean Free Path Contributions to Thermal Conductivity Measured Using Frequency Domain Thermoreflectance”, *Nature Communications*, vol. 4, no. 1, pp. 1–7, 2013.

14. Asheghi, M., Y. K. Leung, S. S. Wong, and K. E. Goodson, “Phonon-Boundary Scattering in Thin Silicon Layers”, *Applied Physics Letters*, vol. 71, no. 13, pp. 1798–1800, 1997.

15. Cahill, D. G., H. E. Fischer, T. Klitsner, E. T. Swartz, and R. O. Pohl, “Thermal Conductivity of Thin Films: Measurements and Understanding”, *Journal of Vacuum Science & Technology A: Vacuum, Surfaces, and Films*, vol. 7, no. 3, pp. 1259–1266, 1989.

16. Ordonez-Miranda, J., R. Yang, S. Volz, and J. J. Alvarado-Gil, “Steady State and Modulated Heat Conduction in Layered Systems Predicted by The Analytical Solution of

The Phonon Boltzmann Transport Equation", *Journal of Applied Physics*, vol. 118, no. 7, p. 075103, 2015.

17. Müller-Plathe, F., "A Simple Nonequilibrium Molecular Dynamics Method for Calculating the Thermal Conductivity", *The Journal of Chemical Physics*, vol. 106, no. 14, pp. 6082–6085, 1997.

18. Ward, A., D. A. Broido, D. A. Stewart, and G. Deinzer, "Ab Initio Theory of the Lattice Thermal Conductivity in Diamond", *Physical Review B*, vol. 80, no. 12, pp. 1–8, 2009.

19. Xu, Yu., J. S. Wang, W. Duan, B. L. Gu, and B. Li, "Nonequilibrium Green's Function Method for Phonon-Phonon Interactions and Ballistic-Diffusive Thermal Transport", *Physical Review B*, vol. 78, no. 22, pp. 1–9, 2008.

20. Chernatynskiy, A. and S. R. Phillpot, "Evaluation of Computational Techniques for Solving the Boltzmann Transport Equation for Lattice Thermal Conductivity Calculations", *Physical Review B*, vol. 82, no. 13, pp. 1–17, 2010.

21. Jeng, M. S., R. Yang, D. Song, and G. Chen, "Modeling the Thermal Conductivity and Phonon Transport in Nanoparticle Composites Using Monte Carlo Simulation", *Journal of Heat Transfer*, vol. 130, no. 4, pp. 1–11, 2008.

22. Lukes, J. R., D. Y. Li, X. G. Liang, and C. L. Tien, "Molecular Dynamics Study of Solid Thin-Film Thermal Conductivity", *Journal of Heat Transfer*, vol. 122, no. 3, pp. 536–543, 2000.

23. Chen, L., N. Kumari, S. Chen, and Y. Hou, "Thermal Conductivity of Multilayer Dielectric Films from Molecular Dynamics Simulations", *RSC Advances*, vol. 7, no. 42, pp. 26194–26201, 2017.

24. Wang, H. and M. Sen, "Analysis of the 3-Omega Method for Thermal Conductivity Measurement", *International Journal of Heat and Mass Transfer*, vol. 52, no. 7–8, pp. 2102–2109, 2009.

25. Zhu, J., D. Tang, W. Wang, J. Liu, K. W. Holub, and R. Yang, “Ultrafast Thermoreflectance Techniques for Measuring Thermal Conductivity and Interface Thermal Conductance of Thin Films”, *Journal of Applied Physics,* vol. 108, no. 9, 2010.

26. Schmidt, A. J., R. Cheaito, and M. Chiesa, “A Frequency-Domain Thermoreflectance Method for the Characterization of Thermal Properties”, *Review of Scientific Instruments,* vol. 80, no. 9, p. 094901, 2009.

27. Chen, S., Q. Li, Q. Zhang, Y. Qu, H. Ji, R. S. Ruoff, and W. Cai, “Thermal Conductivity Measurements of Suspended Graphene with and without Wrinkles by Micro-Raman Mapping”, *Nanotechnology*, vol. 23, no. 36, p. 365701, 2012.

28. Luo, Z., H. Liu, B. T. Spann, Y. Feng, P. Ye, Y. P. Chen, and X. Xu, “Measurement of in-Plane Thermal Conductivity of Ultrathin Films Using Micro-Raman Spectroscopy”, *Nanoscale and Microscale Thermophysical Engineering*, vol. 18, no. 2, pp. 183–193, 2014.

29. Huang, S., Y. Chen, Z. Luo, and X. Xu, “Temperature and Strain Effects in Micro-Raman Thermometry for Measuring in-Plane Thermal Conductivity of Thin Films”, *Nanoscale and Microscale Thermophysical Engineering*, vol. 25, no. 2, pp. 91–100, 2021.

30. Sahoo, S., S. K. Mallik, M. C. Sahu, A. Joseph, S. Singh, S. K. Gupta, B. Rout, G. K. Pradhan, and S. Sahoo, “Thermal Conductivity of Free-Standing Silicon Thermal Conductivity of Free-Standing Silicon Nanowire Using Raman”, *Nanotechnology*, vol. 31, no 50, p. 505701, 2020.

31. Ember, K. J. I., M. A. Hoeve, S. L. McAughtrie, M. S. Bergholt, B. J. Dwyer, M. M. Stevens, K. Faulds, S. J. Forbes, and C. J. Campbell, “Raman Spectroscopy and Regenerative Medicine: A Review”, *NPJ Regenerative Medicine*, vol. 2, no. 1, pp 1-10, 2017.

32. Hossain, M. T. and P. K. Giri, “Temperature-Dependent Raman Studies and Thermal Conductivity of Direct CVD Grown Non-Van Der Waals Layered Bi2O2Se”, *Journal of Applied Physics*, vol. 129, no. 17, p. 175102, 2021.

33. Beechem, T., L. Yates, and S. Graham, “Invited Review Article : Error and Uncertainty in Raman Thermal Conductivity Measurements”, *Review of Scientific Instruments*, vol. 86, no. 4, pp. 1–12, 2015.

34. Donmezer, F. N., D. Singh, W. James, A. Christensen, S. Graham, and J.Y. Murthy, “Lattice Boltzmann and Discrete Ordinates Methods for Phonon Transport Modeling: A Comparative Study”, *ASME International Mechanical Engineering Congress and Exposition*, vol. 54969, pp. 333–343, 2011.

35. Mazumder, S. and A. Majumdar, “Monte Carlo Study of Phonon Transport in Solid Thin Films Including Dispersion and Polarization”, *Journal of Heat Transfer*, vol. 123, no. 4, pp. 749–759, 2001.

36. Donmezer, N., and S. Graham, “A Multiscale Thermal Modeling Approach for Ballistic and Diffusive Heat Transport in Two Dimensional Domains”, *International Journal of Thermal Sciences*, vol. 76, pp. 235–244, 2014.

37. Hua, Y. C. and B. Y. Cao, “The Effective Thermal Conductivity of Ballistic-Diffusive Heat Conduction in Nanostructures with Internal Heat Source”, *International Journal of Heat and Mass Transfer*, vol. 92, pp. 995–1003, 2016.

38. Woodrow, A. F., 1991, *The Selection of Discrete Ordinate Quadrature Sets for Anisotropic Scattering*, American Society of Mechanical Engineers (ASME) Heat Transfer Division (HTD).

39. Zeng, L., K. C. Collins, Y. Hu, M. N. Luckyanova, A. A. Maznev, S. Huberman, V. Chiloyan, J. Zhou, X. Huang, K. A. Nelson, and G. Chen, “Measuring Phonon Mean Free Path Distributions by Probing Quasiballistic Phonon Transport in Grating Nanostructures”, *Scientific Reports*, vol. 5, no. 1, pp. 1–10, 2015.

40. Hua, C. and A. J. Minnich, “Semi-Analytical Solution to the Frequency-Dependent Boltzmann Transport Equation for Cross-Plane Heat Conduction in Thin Films”, *Journal of Applied Physics*, vol. 117, no. 17, p. 175306, 2015.

41. Bao, H., J. Chen, X. Gu, and B. Cao, "A Review of Simulation Methods in Micro/Nanoscale Heat Conduction", *ES Energy & Environment*, vol. 1, no. 34, pp. 16-55, 2018.

42. Luo, T., J. Garg, J. Shiomi, K. Esfarjani, and G. Chen, "Gallium Arsenide Thermal Conductivity and Optical Phonon Relaxation Times from First-Principles Calculations", *EPL (Europhysics Letters)*, vol. 101, no. 1, p. 16001, 2013.

43. Freedman, J. P., J. H. Leach, E. A. Preble, Z. Sitar, R. F. Davis, and J. A. Malen, "Universal Phonon Mean Free Path Spectra in Crystalline Semiconductors at High Temperature", *Scientific Reports*, vol. 3, no. 1, pp. 1–6, 2013.

44. Beechem, T. E., A. E. McDonald, E. J. Fuller, A. A. Talin, C. M. Rost, J. P. Maria, J. T. Gaskins, P. E. Hopkins, and A. A. Allerman, "Size Dictated Thermal Conductivity of GaN", *Journal of Applied Physics*, vol. 120, no. 9, p. 095104, 2017.

45. Gholivand, H. and N. Donmezer, "Phonon Mean Free Path in Few Layer Graphene, Hexagonal Boron Nitride, and Composite Bilayer h-BN/Graphene", *IEEE Transactions on Nanotechnology*, vol. 16, no. 5, pp. 752–758, 2017.

46. Capinski, W. S. and H. J. Maris, "Thermal Conductivity of GaAs/AlAs Superlattices", *Physica B: Condensed Matter*, vol. 219, pp. 699–701, 1996.

47. Liu, W. and M. Ashegi, "Thermal Conductivity Measurements of Ultra-Thin Single Crystal Silicon Layers", *Journal of Heat Transfer*, vol. 128, no.1, pp. 75–83, 2006.

48. Killat, N., M. Montes, J. W. Pomeroy, T. Paskova, K. R. Evans, J. Leach, X. Li, U. Ozgur, H. Morkoc, K.D. Chabak, and A. Crespo, "Thermal Properties of AlGaN / GaN HFETs on Bulk GaN Substrates", *IEEE Electron Device Letters*, vol. 33, no. 3, pp. 366–368, 2012.

49. Lee, J., D. Yoon, H. Kim, S. W. Lee, and H. Cheong, "Thermal Conductivity of Suspended Pristine Graphene Measured by Raman Spectroscopy", *Physical Review B*, vol. 83, no. 8, pp. 1–4, 2011.

50. Glazov, V. M. and A. S. Pashinkin, “Thermal Expansion and Heat Capacity of GaAs and InAs,” *Inorganic Materials*, vol. 36, no. 3, pp. 225–231, 2000.

51. Zhang, Y., J. X. Cao, Y. Xiao, and X. H. Yan, “Phonon Spectrum and Specific Heat of Silicon Nanowires”, *Journal of Applied Physics*, vol. 102, no. 10, p. 104303, 2007.

52. Sanati, M. and S. K. Estreicher, “Specific Heat and Entropy of GaN”, *Journal of Physics: Condensed Matter*, vol. 16, no. 28, p. L327, 2004.

53. Kostecki, M., T. Cygan, M. Petrus, and J. Jaroszewicz, “Thermal Properties of Multilayer Graphene and HBN Reinforced Copper Matrix Composites”, *Journal of Thermal Analysis and Calorimetry*, vol. 138, no. 6, pp. 3873–3883, 2019.

54. Lekner, J., 1987, *Theory of Reflection of Electromagnetic and Particle Waves*, Springer Science and Business Media.

55. Kim D. J. and J. W. Kim, “High-Power TEM00 and Laguerre–Gaussian Mode Generation in Double Resonator Configuration”, *Applied Physics B*, vol. 121, no. 3, pp. 401–405, 2015.

56. Łęcka, K. M., J. Gąsiorek, A. Mazur-Nowacka, B. Szczygieł, and A. J. Antończak, “Adhesion and Corrosion Resistance of Laser-Oxidized Titanium in Potential Biomedical Application”, *Surface and Coatings Technology*, vol. 366, pp. 179–189, 2019.

57. Jellison Jr., G. E, “Optical Functions of GaAs, GaP, and Ge Determined by Two-Channel Polarization Modulation Ellipsometry”, *Optical Materials*, vol. 1, no. 3, pp. 151–160, 1992.

58. Aspnes, D. E. and A. A. Studna, “Dielectric Functions and Optical Parameters of Si, Ge, GaP, GaAs, GaSb, InP, InAs, and InSb from 1.5 to 6.0 eV”, *Physical Review B*, vol. 27, no. 2, p. 985, 1983.

59. Kawashima, T., H. Yoshikawa, and S. Adachi, “Optical Properties of Hexagonal GaN”, *Journal of Applied Physics*, vol. 82, no. 7, pp. 3528-3535, 1997.

60. Larruquert, JI., L. V. Rodríguez-de Marcos, J. A. Méndez, P. J. Martin, and A. Bendavid, "High Reflectance Ta-C Coatings in the Extreme Ultraviolet", *Optics Express*, vol. 21, no. 23, pp. 27537-27549, 2013.

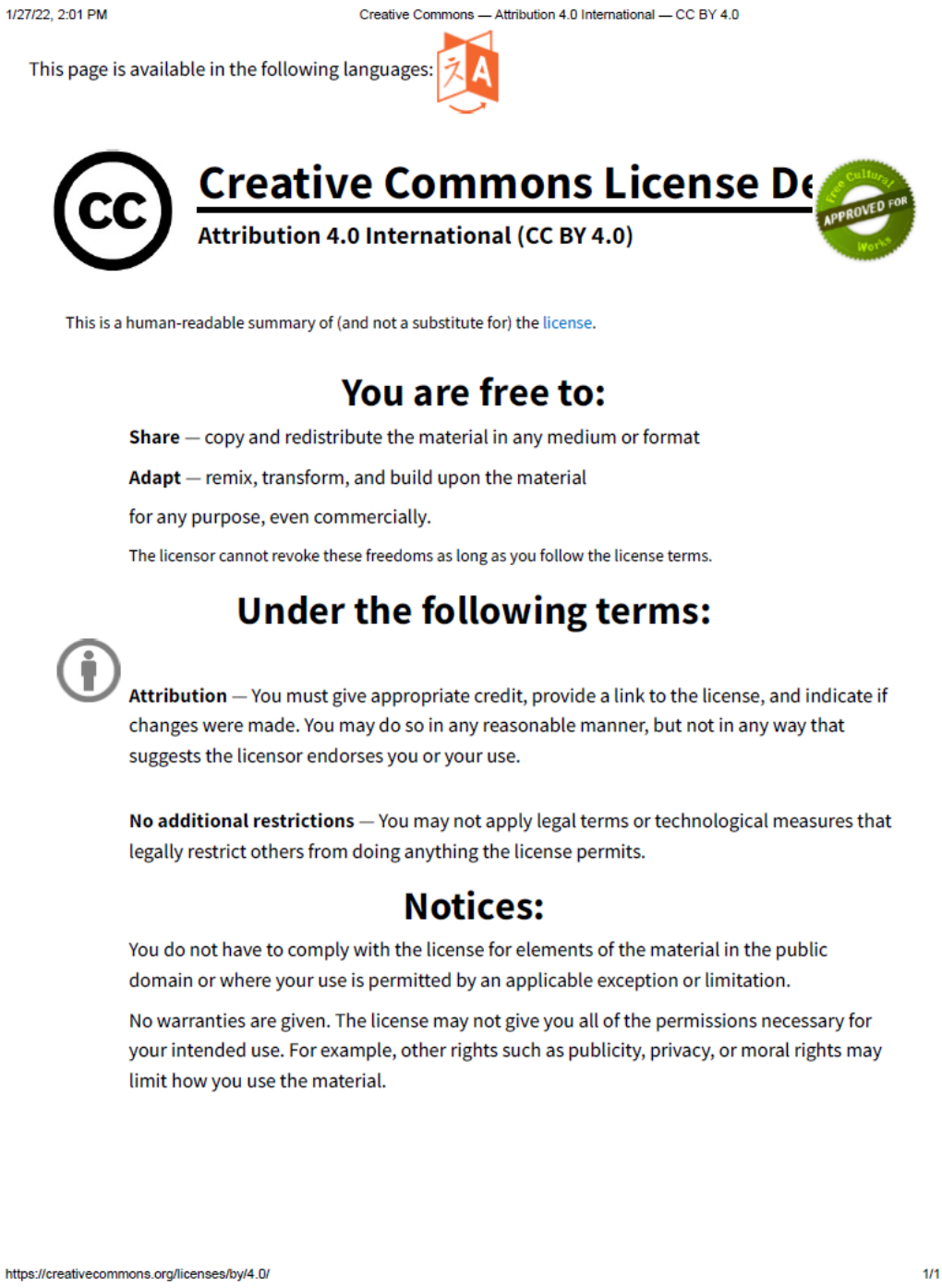
61. Papatryfonos, K., T. Angelova, A. Brimont, B. Reid, S. Guldin, P. R. Smith, M. Tang, K. Li, A. J. Seeds, H. Liu, and D. R. Selviah, "Refractive Indices of MBE-Grown $Al_xGa_{(1-x)}$ As Ternary Alloys in the Transparent Wavelength Region", *AIP Advances*, vol. 11, no. 2, p. 025327, 2021.

62. Green, M. A., "Self-Consistent Optical Parameters of Intrinsic Silicon at 300K Including Temperature Coefficient", *Solar Energy Materials and Solar Cells*, vol. 92, no. 11, pp. 1305–1310, 2008.

63. Barker JR., A. S. and M. Ilegems, "Infrared Lattice Vibrations and Free-Electron Dispersion in GaN", *Physical Review B*, vol. 7, no. 2, p.743, 1973.

64. Weber, J. W., V. E. Calado, and M. C. M. Van De Sanden, "Optical Constants of Graphene Measured by Spectroscopic Ellipsometry", *Applied Physics Letters*, vol. 97, no. 9, pp. 1–4, 2010.

APPENDIX A: COPYRIGHT PERMISSIONS



1/27/22, 2:01 PM Creative Commons — Attribution 4.0 International — CC BY 4.0

This page is available in the following languages:

Creative Commons License De

Attribution 4.0 International (CC BY 4.0)

This is a human-readable summary of (and not a substitute for) the license.

You are free to:

Share — copy and redistribute the material in any medium or format

Adapt — remix, transform, and build upon the material

for any purpose, even commercially.

The licensor cannot revoke these freedoms as long as you follow the license terms.

Under the following terms:

Attribution — You must give appropriate credit, provide a link to the license, and indicate if changes were made. You may do so in any reasonable manner, but not in any way that suggests the licensor endorses you or your use.

No additional restrictions — You may not apply legal terms or technological measures that legally restrict others from doing anything the license permits.

Notices:

You do not have to comply with the license for elements of the material in the public domain or where your use is permitted by an applicable exception or limitation.

No warranties are given. The license may not give you all of the permissions necessary for your intended use. For example, other rights such as publicity, privacy, or moral rights may limit how you use the material.

https://creativecommons.org/licenses/by/4.0/ 1/1

Figure A.1. Copyright permission for Figure 1.1.



1/27/22, 2:05 PM Rightslink® by Copyright Clearance Center

CCC RightsLink®

Home | Help | Live Chat | Sign In | Create Account

IEEE Requesting permission to reuse content from an IEEE publication

Improved Light Output Power of InGaN/GaN LED by Using Ultrasonic Spray Pyrolysis Deposited MgO

Author: Han-Yin Liu
Publication: IEEE Transactions on Electron Devices
Publisher: IEEE
Date: Aug. 2017

Copyright © 2017, IEEE

Thesis / Dissertation Reuse

The IEEE does not require individuals working on a thesis to obtain a formal reuse license, however, you may print out this statement to be used as a permission grant:

Requirements to be followed when using any portion (e.g., figure, graph, table, or textual material) of an IEEE copyrighted paper in a thesis:

1) In the case of textual material (e.g., using short quotes or referring to the work within these papers) users must give full credit to the original source (author, paper, publication) followed by the IEEE copyright line © 2011 IEEE.
2) In the case of illustrations or tabular material, we require that the copyright line © [Year of original publication] IEEE appear prominently with each reprinted figure and/or table.
3) If a substantial portion of the original paper is to be used, and if you are not the senior author, also obtain the senior author's approval.

Requirements to be followed when using an entire IEEE copyrighted paper in a thesis:

1) The following IEEE copyright/ credit notice should be placed prominently in the references: © [year of original publication] IEEE. Reprinted, with permission, from [author names, paper title, IEEE publication title, and month/year of publication]
2) Only the accepted version of an IEEE copyrighted paper can be used when posting the paper or your thesis on-line.
3) In placing the thesis on the author's university website, please display the following message in a prominent place on the website: In reference to IEEE copyrighted material which is used with permission in this thesis, the IEEE does not endorse any of [university/educational entity's name goes here]'s products or services. Internal or personal use of this material is permitted. If interested in reprinting/republishing IEEE copyrighted material for advertising or promotional purposes or for creating new collective works for resale or redistribution, please go to http://www.ieee.org/publications_standards/publications/rights/rights_link.html to learn how to obtain a License from RightsLink.

If applicable, University Microfilms and/or ProQuest Library, or the Archives of Canada may supply single copies of the dissertation.

BACK CLOSE WINDOW

© 2022 Copyright - All Rights Reserved | Copyright Clearance Center, Inc. | Privacy statement | Terms and Conditions
Comments? We would like to hear from you. E-mail us at customercare@copyright.com

Figure A.2. Copyright permission for Figure 1.2.

AIP PUBLISHING LICENSE
TERMS AND CONDITIONS

Jan 27, 2022

This Agreement between Bogazici University -- Taher Meydando ("You") and AIP Publishing ("AIP Publishing") consists of your license details and the terms and conditions provided by AIP Publishing and Copyright Clearance Center.

License Number	5237020572679
License date	Jan 27, 2022
Licensed Content Publisher	AIP Publishing
Licensed Content Publication	Journal of Applied Physics
Licensed Content Title	Nanoscale electro-thermal interactions in AlGaN/GaN high electron mobility transistors
Licensed Content Author	Bikramjit Chatterjee, Canberk Dundar, Thomas E. Beechem, et al
Licensed Content Date	Jan 31, 2020
Licensed Content Volume	127
Licensed Content Issue	4
Type of Use	Thesis/Dissertation
Requestor type	University or Educational Institution

Figure A.3. Copyright permission for Figure 1.3.

Format	Print and electronic
Portion	Figure/Table
Number of figures/tables	1
Will you be translating?	No
Title	Modified Numerical Method for Thin Film Thermal Conductivity Calculation with Micro-Raman Spectroscopy
Institution name	Bogazici University
Expected presentation date	Jan 2022
Order reference number	123123
Portions	Figure 1. (c)
Requestor Location	Bogazici University Bebek/Besiktas Istanbul, 34342 Turkey Attn: Bogazici University
Total	0.00 USD

Terms and Conditions

AIP Publishing -- Terms and Conditions: Permissions Uses

AIP Publishing hereby grants to you the non-exclusive right and license to use and/or distribute the Material according to the use specified in your order, on a one-time basis, for the specified term, with a maximum distribution equal to the number that you have ordered. Any links or other content accompanying the Material are not the subject of this license.

Figure A.3. Copyright permission for Figure 1.3 (cont.).

1. You agree to include the following copyright and permission notice with the reproduction of the Material:"Reprinted from [FULL CITATION], with the permission of AIP Publishing." For an article, the credit line and permission notice must be printed on the first page of the article or book chapter. For photographs, covers, or tables, the notice may appear with the Material, in a footnote, or in the reference list.
2. If you have licensed reuse of a figure, photograph, cover, or table, it is your responsibility to ensure that the material is original to AIP Publishing and does not contain the copyright of another entity, and that the copyright notice of the figure, photograph, cover, or table does not indicate that it was reprinted by AIP Publishing, with permission, from another source. Under no circumstances does AIP Publishing purport or intend to grant permission to reuse material to which it does not hold appropriate rights.
   You may not alter or modify the Material in any manner. You may translate the Material into another language only if you have licensed translation rights. You may not use the Material for promotional purposes.
3. The foregoing license shall not take effect unless and until AIP Publishing or its agent, Copyright Clearance Center, receives the Payment in accordance with Copyright Clearance Center Billing and Payment Terms and Conditions, which are incorporated herein by reference.
4. AIP Publishing or Copyright Clearance Center may, within two business days of granting this license, revoke the license for any reason whatsoever, with a full refund payable to you. Should you violate the terms of this license at any time, AIP Publishing, or Copyright Clearance Center may revoke the license with no refund to you. Notice of such revocation will be made using the contact information provided by you. Failure to receive such notice will not nullify the revocation.
5. AIP Publishing makes no representations or warranties with respect to the Material. You agree to indemnify and hold harmless AIP Publishing, and their officers, directors, employees or agents from and against any and all claims arising out of your use of the Material other than as specifically authorized herein.
6. The permission granted herein is personal to you and is not transferable or assignable without the prior written permission of AIP Publishing. This license may not be amended except in a writing signed by the party to be charged.
7. If purchase orders, acknowledgments or check endorsements are issued on any forms containing terms and conditions which are inconsistent with these provisions, such inconsistent terms and conditions shall be of no force and effect. This document, including the CCC Billing and Payment Terms and Conditions, shall be the entire agreement between the parties relating to the subject matter hereof.

This Agreement shall be governed by and construed in accordance with the laws of the State of New York. Both parties hereby submit to the jurisdiction of the courts of New York County for purposes of resolving any disputes that may arise hereunder.

V1.2

Questions? customercare@copyright.com or +1-855-239-3415 (toll free in the US) or +1-978-646-2777.

Figure A.3. Copyright permission for Figure 1.3 (cont.).

AIP PUBLISHING LICENSE
TERMS AND CONDITIONS

Jan 27, 2022

This Agreement between Bogazici University -- Taher Meydando ("You") and AIP Publishing ("AIP Publishing") consists of your license details and the terms and conditions provided by AIP Publishing and Copyright Clearance Center.

License Number	5237020398417
License date	Jan 27, 2022
Licensed Content Publisher	AIP Publishing
Licensed Content Publication	Journal of Applied Physics
Licensed Content Title	Steady state and modulated heat conduction in layered systems predicted by the analytical solution of the phonon Boltzmann transport equation
Licensed Content Author	Jose Ordonez-Miranda, Ronggui Yang, Sebastian Volz, et al
Licensed Content Date	Aug 21, 2015
Licensed Content Volume	118
Licensed Content Issue	7

Figure A.4. Copyright permission for Figure 1.4.

Type of Use	Thesis/Dissertation
Requestor type	University or Educational Institution
Format	Print and electronic
Portion	Figure/Table
Number of figures/tables	1
Will you be translating?	No
Title	Modified Numerical Method for Thin Film Thermal Conductivity Calculation with Micro-Raman Spectroscopy
Institution name	Bogazici University
Expected presentation date	Jan 2022
Order reference number	123123
Portions	Figure 1
Requestor Location	Bogazici University Bebek/Besiktas Istanbul, 34342 Turkey Attn: Bogazici University
Total	0.00 USD

Terms and Conditions

Figure A.4. Copyright permission for Figure 1.4 (cont.).

AIP Publishing -- Terms and Conditions: Permissions Uses

AIP Publishing hereby grants to you the non-exclusive right and license to use and/or distribute the Material according to the use specified in your order, on a one-time basis, for the specified term, with a maximum distribution equal to the number that you have ordered. Any links or other content accompanying the Material are not the subject of this license.

1. You agree to include the following copyright and permission notice with the reproduction of the Material:"Reprinted from [FULL CITATION], with the permission of AIP Publishing." For an article, the credit line and permission notice must be printed on the first page of the article or book chapter. For photographs, covers, or tables, the notice may appear with the Material, in a footnote, or in the reference list.
2. If you have licensed reuse of a figure, photograph, cover, or table, it is your responsibility to ensure that the material is original to AIP Publishing and does not contain the copyright of another entity, and that the copyright notice of the figure, photograph, cover, or table does not indicate that it was reprinted by AIP Publishing, with permission, from another source. Under no circumstances does AIP Publishing purport or intend to grant permission to reuse material to which it does not hold appropriate rights.
   You may not alter or modify the Material in any manner. You may translate the Material into another language only if you have licensed translation rights. You may not use the Material for promotional purposes.
3. The foregoing license shall not take effect unless and until AIP Publishing or its agent, Copyright Clearance Center, receives the Payment in accordance with Copyright Clearance Center Billing and Payment Terms and Conditions, which are incorporated herein by reference.
4. AIP Publishing or Copyright Clearance Center may, within two business days of granting this license, revoke the license for any reason whatsoever, with a full refund payable to you. Should you violate the terms of this license at any time, AIP Publishing, or Copyright Clearance Center may revoke the license with no refund to you. Notice of such revocation will be made using the contact information provided by you. Failure to receive such notice will not nullify the revocation.
5. AIP Publishing makes no representations or warranties with respect to the Material. You agree to indemnify and hold harmless AIP Publishing, and their officers, directors, employees or agents from and against any and all claims arising out of your use of the Material other than as specifically authorized herein.
6. The permission granted herein is personal to you and is not transferable or assignable without the prior written permission of AIP Publishing. This license may not be amended except in a writing signed by the party to be charged.
7. If purchase orders, acknowledgments or check endorsements are issued on any forms containing terms and conditions which are inconsistent with these provisions, such inconsistent terms and conditions shall be of no force and effect. This document, including the CCC Billing and Payment Terms and Conditions, shall be the entire agreement between the parties relating to the subject matter hereof.

This Agreement shall be governed by and construed in accordance with the laws of the State of New York. Both parties hereby submit to the jurisdiction of the courts of New York County for purposes of resolving any disputes that may arise hereunder.

V1.2

Questions? customercare@copyright.com or +1-855-239-3415 (toll free in the US) or

Figure A.4. Copyright permission for Figure 1.4 (cont.).

+1-978-646-2777.

Figure A.4. Copyright permission for Figure 1.4 (cont.).

CCC Marketplace™

This is a License Agreement between Taher Meydando ("User") and Copyright Clearance Center, Inc. ("CCC") on behalf of the Rightsholder identified in the order details below. The license consists of the order details, the CCC Terms and Conditions below, and any Rightsholder Terms and Conditions which are included below.

All payments must be made in full to CCC in accordance with the CCC Terms and Conditions below.

Order Date	27-Jan-2022	Type of Use	Republish in a thesis/dissertation
Order License ID	1182888-1		
ISSN	2046-2069	Publisher	RSC Publishing
		Portion	Image/photo/illustration

LICENSED CONTENT

Publication Title	RSC advances	Publication Type	e-Journal
Article Title	Thermal conductivity of multilayer dielectric films from molecular dynamics simulations	Start Page	26194
		End Page	26201
		Issue	42
Date	01/01/2011	Volume	7
Language	English	URL	http://pubs.rsc.org/en/Journals/JournalIssues/RA
Country	United Kingdom of Great Britain and Northern Ireland		
Rightsholder	Royal Society of Chemistry		

REQUEST DETAILS

Portion Type	Image/photo/illustration	Distribution	Worldwide
Number of images / photos / illustrations	1	Translation	Original language of publication
Format (select all that apply)	Print, Electronic	Copies for the disabled?	No
		Minor editing privileges?	No
Who will republish the content?	Academic institution	Incidental promotional use?	No
Duration of Use	Current edition and up to 5 years	Currency	USD
Lifetime Unit Quantity	Up to 499		
Rights Requested	Main product		

NEW WORK DETAILS

Title	Modified Numerical Method for Thin Film Thermal Conductivity Calculation with Micro-Raman Spectroscopy	Institution name	Bogazici University
		Expected presentation date	2022-01-27
Instructor name	Taher Meydando		

ADDITIONAL DETAILS

Figure A.5. Copyright permission for Figure 1.5.

Order reference number	N/A	**The requesting person / organization to appear on the license**	Taher Meydando

REUSE CONTENT DETAILS

Title, description or numeric reference of the portion(s)	Schematic of lattice structures in NEMD simulations	**Title of the article/chapter the portion is from**	Thermal conductivity of multilayer dielectric films from molecular dynamics simulations
Editor of portion(s)	Chen, Liang; Kumari, Niru; Chen, Shuangtao; Hou, Yu	**Author of portion(s)**	Chen, Liang; Kumari, Niru; Chen, Shuangtao; Hou, Yu
Volume of serial or monograph	7	**Issue, if republishing an article from a serial**	42
Page or page range of portion	26194-26201	**Publication date of portion**	2017-05-15

CCC Terms and Conditions

1. Description of Service; Defined Terms. This Republication License enables the User to obtain licenses for republication of one or more copyrighted works as described in detail on the relevant Order Confirmation (the "Work(s)"). Copyright Clearance Center, Inc. ("CCC") grants licenses through the Service on behalf of the rightsholder identified on the Order Confirmation (the "Rightsholder"). "Republication", as used herein, generally means the inclusion of a Work, in whole or in part, in a new work or works, also as described on the Order Confirmation. "User", as used herein, means the person or entity making such republication.

2. The terms set forth in the relevant Order Confirmation, and any terms set by the Rightsholder with respect to a particular Work, govern the terms of use of Works in connection with the Service. By using the Service, the person transacting for a republication license on behalf of the User represents and warrants that he/she/it (a) has been duly authorized by the User to accept, and hereby does accept, all such terms and conditions on behalf of User, and (b) shall inform User of all such terms and conditions. In the event such person is a "freelancer" or other third party independent of User and CCC, such party shall be deemed jointly a "User" for purposes of these terms and conditions. In any event, User shall be deemed to have accepted and agreed to all such terms and conditions if User republishes the Work in any fashion.

3. Scope of License; Limitations and Obligations.

    3.1. All Works and all rights therein, including copyright rights, remain the sole and exclusive property of the Rightsholder. The license created by the exchange of an Order Confirmation (and/or any invoice) and payment by User of the full amount set forth on that document includes only those rights expressly set forth in the Order Confirmation and in these terms and conditions, and conveys no other rights in the Work(s) to User. All rights not expressly granted are hereby reserved.

    3.2. General Payment Terms: You may pay by credit card or through an account with us payable at the end of the month. If you and we agree that you may establish a standing account with CCC, then the following terms apply: Remit Payment to: Copyright Clearance Center, 29118 Network Place, Chicago, IL 60673-1291. Payments Due: Invoices are payable upon their delivery to you (or upon our notice to you that they are available to you for downloading). After 30 days, outstanding amounts will be subject to a service charge of 1-1/2% per month or, if less, the maximum rate allowed by applicable law. Unless otherwise specifically set forth in the Order Confirmation or in a separate written agreement signed by CCC, invoices are due and payable on "net 30" terms. While User may exercise the rights licensed immediately upon issuance of the Order Confirmation, the license is automatically revoked and is null and void, as if it had never been issued, if complete payment for the license is not received on a timely basis either from User directly or through a payment agent, such as a credit card company.

Figure A.5. Copyright permission for Figure 1.5 (cont.).

3.3. Unless otherwise provided in the Order Confirmation, any grant of rights to User (i) is "one-time" (including the editions and product family specified in the license), (ii) is non-exclusive and non-transferable and (iii) is subject to any and all limitations and restrictions (such as, but not limited to, limitations on duration of use or circulation) included in the Order Confirmation or invoice and/or in these terms and conditions. Upon completion of the licensed use, User shall either secure a new permission for further use of the Work(s) or immediately cease any new use of the Work(s) and shall render inaccessible (such as by deleting or by removing or severing links or other locators) any further copies of the Work (except for copies printed on paper in accordance with this license and still in User's stock at the end of such period).

3.4. In the event that the material for which a republication license is sought includes third party materials (such as photographs, illustrations, graphs, inserts and similar materials) which are identified in such material as having been used by permission, User is responsible for identifying, and seeking separate licenses (under this Service or otherwise) for, any of such third party materials; without a separate license, such third party materials may not be used.

3.5. Use of proper copyright notice for a Work is required as a condition of any license granted under the Service. Unless otherwise provided in the Order Confirmation, a proper copyright notice will read substantially as follows: "Republished with permission of [Rightsholder's name], from [Work's title, author, volume, edition number and year of copyright]; permission conveyed through Copyright Clearance Center, Inc. " Such notice must be provided in a reasonably legible font size and must be placed either immediately adjacent to the Work as used (for example, as part of a by-line or footnote but not as a separate electronic link) or in the place where substantially all other credits or notices for the new work containing the republished Work are located. Failure to include the required notice results in loss to the Rightsholder and CCC, and the User shall be liable to pay liquidated damages for each such failure equal to twice the use fee specified in the Order Confirmation, in addition to the use fee itself and any other fees and charges specified.

3.6. User may only make alterations to the Work if and as expressly set forth in the Order Confirmation. No Work may be used in any way that is defamatory, violates the rights of third parties (including such third parties' rights of copyright, privacy, publicity, or other tangible or intangible property), or is otherwise illegal, sexually explicit or obscene. In addition, User may not conjoin a Work with any other material that may result in damage to the reputation of the Rightsholder. User agrees to inform CCC if it becomes aware of any infringement of any rights in a Work and to cooperate with any reasonable request of CCC or the Rightsholder in connection therewith.

4. Indemnity. User hereby indemnifies and agrees to defend the Rightsholder and CCC, and their respective employees and directors, against all claims, liability, damages, costs and expenses, including legal fees and expenses, arising out of any use of a Work beyond the scope of the rights granted herein, or any use of a Work which has been altered in any unauthorized way by User, including claims of defamation or infringement of rights of copyright, publicity, privacy or other tangible or intangible property.

5. Limitation of Liability. UNDER NO CIRCUMSTANCES WILL CCC OR THE RIGHTSHOLDER BE LIABLE FOR ANY DIRECT, INDIRECT, CONSEQUENTIAL OR INCIDENTAL DAMAGES (INCLUDING WITHOUT LIMITATION DAMAGES FOR LOSS OF BUSINESS PROFITS OR INFORMATION, OR FOR BUSINESS INTERRUPTION) ARISING OUT OF THE USE OR INABILITY TO USE A WORK, EVEN IF ONE OF THEM HAS BEEN ADVISED OF THE POSSIBILITY OF SUCH DAMAGES. In any event, the total liability of the Rightsholder and CCC (including their respective employees and directors) shall not exceed the total amount actually paid by User for this license. User assumes full liability for the actions and omissions of its principals, employees, agents, affiliates, successors and assigns.

6. Limited Warranties. THE WORK(S) AND RIGHT(S) ARE PROVIDED "AS IS". CCC HAS THE RIGHT TO GRANT TO USER THE RIGHTS GRANTED IN THE ORDER CONFIRMATION DOCUMENT. CCC AND THE RIGHTSHOLDER DISCLAIM ALL OTHER WARRANTIES RELATING TO THE WORK(S) AND RIGHT(S), EITHER EXPRESS OR IMPLIED, INCLUDING WITHOUT LIMITATION IMPLIED WARRANTIES OF MERCHANTABILITY OR FITNESS FOR A PARTICULAR PURPOSE. ADDITIONAL RIGHTS MAY BE REQUIRED TO USE ILLUSTRATIONS, GRAPHS, PHOTOGRAPHS, ABSTRACTS, INSERTS OR OTHER PORTIONS OF THE WORK (AS OPPOSED TO THE ENTIRE WORK) IN A MANNER CONTEMPLATED BY USER;

Figure A.5. Copyright permission for Figure 1.5 (cont.).

USER UNDERSTANDS AND AGREES THAT NEITHER CCC NOR THE RIGHTSHOLDER MAY HAVE SUCH ADDITIONAL RIGHTS TO GRANT.

7. Effect of Breach. Any failure by User to pay any amount when due, or any use by User of a Work beyond the scope of the license set forth in the Order Confirmation and/or these terms and conditions, shall be a material breach of the license created by the Order Confirmation and these terms and conditions. Any breach not cured within 30 days of written notice thereof shall result in immediate termination of such license without further notice. Any unauthorized (but licensable) use of a Work that is terminated immediately upon notice thereof may be liquidated by payment of the Rightsholder's ordinary license price therefor; any unauthorized (and unlicensable) use that is not terminated immediately for any reason (including, for example, because materials containing the Work cannot reasonably be recalled) will be subject to all remedies available at law or in equity, but in no event to a payment of less than three times the Rightsholder's ordinary license price for the most closely analogous licensable use plus Rightsholder's and/or CCC's costs and expenses incurred in collecting such payment.

8. Miscellaneous.

   8.1. User acknowledges that CCC may, from time to time, make changes or additions to the Service or to these terms and conditions, and CCC reserves the right to send notice to the User by electronic mail or otherwise for the purposes of notifying User of such changes or additions; provided that any such changes or additions shall not apply to permissions already secured and paid for.

   8.2. Use of User-related information collected through the Service is governed by CCC's privacy policy, available online here:https://marketplace.copyright.com/rs-ui-web/mp/privacy-policy

   8.3. The licensing transaction described in the Order Confirmation is personal to User. Therefore, User may not assign or transfer to any other person (whether a natural person or an organization of any kind) the license created by the Order Confirmation and these terms and conditions or any rights granted hereunder; provided, however, that User may assign such license in its entirety on written notice to CCC in the event of a transfer of all or substantially all of User's rights in the new material which includes the Work(s) licensed under this Service.

   8.4. No amendment or waiver of any terms is binding unless set forth in writing and signed by the parties. The Rightsholder and CCC hereby object to any terms contained in any writing prepared by the User or its principals, employees, agents or affiliates and purporting to govern or otherwise relate to the licensing transaction described in the Order Confirmation, which terms are in any way inconsistent with any terms set forth in the Order Confirmation and/or in these terms and conditions or CCC's standard operating procedures, whether such writing is prepared prior to, simultaneously with or subsequent to the Order Confirmation, and whether such writing appears on a copy of the Order Confirmation or in a separate instrument.

   8.5. The licensing transaction described in the Order Confirmation document shall be governed by and construed under the law of the State of New York, USA, without regard to the principles thereof of conflicts of law. Any case, controversy, suit, action, or proceeding arising out of, in connection with, or related to such licensing transaction shall be brought, at CCC's sole discretion, in any federal or state court located in the County of New York, State of New York, USA, or in any federal or state court whose geographical jurisdiction covers the location of the Rightsholder set forth in the Order Confirmation. The parties expressly submit to the personal jurisdiction and venue of each such federal or state court.If you have any comments or questions about the Service or Copyright Clearance Center, please contact us at 978-750-8400 or send an e-mail to support@copyright.com.

v 1.1

Figure A.5. Copyright permission for Figure 1.5 (cont.).

Scientific Research (//www.scirp.org)
An Academic Publisher

OPEN ACCESS
(/journal/openaccess.aspx)

Home (../index.aspx) > Journals (index.aspx) > Cite this Article

Search Title, Keywords, Author, etc.

OJPC (home.aspx?journalid=589)> Vol.2 No.1, February 2012 (home.aspx?issueid=1427#17521)

Open Journal of Physical Chemistry
Vol.2 No.1(2012), Paper ID 17521, 6 pages
DOI:10.4236/ojpc.2012.21001 (http://dx.doi.org/10.4236/ojpc.2012.21001)

Study of Thermal Conductivity of Porous Silicon Using the Micro-Raman Method

Amaria Ould-Abbas, Mama Bouchaour, Nasr-Eddine Chabane Sari

• Abstract (paperinformation.aspx?paperid=17521&#abstract)
• Full-Text PDF (//www.scirp.org/pdf/OJPC201
• Full-Text HTML (//www.scirp.org/html/1-1230011_17521.htm)
• Linked References (paperinformation.aspx?paperid=17521#reference)
• How to Cite this Article (cta.aspx?paperid=17521)

Research Unit Materials and Renewable Energy (RUMRE), University of Abou Bekr BELKAID of Tlemcen, Tlemcen, Algeria

Copyright © 2012 Amaria Ould-Abbas, Mama Bouchaour, Nasr-Eddine Chabane Sari et al. This is an open access article distributed under the Creative Commons Attribution License, which permits unrestricted use, distribution, and reproduction in any medium, provided the original work is properly cited.

How to Cite this Article

A. Ould-Abbas, M. Bouchaour and N. Sari, "Study of Thermal Conductivity of Porous Silicon Using the Micro-Raman Method," *Open Journal of Physical Chemistry*, Vol. 2 No. 1, 2012, pp. 1-6. doi: 10.4236/ojpc.2012.21001 (http://dx.doi.org/10.4236/ojpc.2012.21001).

Download citation as EndNote

Journals Menu

Related Articles

- Thermal Conductivity and Microstructure Properties of Porous SiC Ceramic Derived from Silicon Carbide Powder (paperinformation.aspx?paperid=27346)
- Silicon Nanocrystals on the Surface of Standard Si Wafers: A Micro-Raman Investigation (paperinformation.aspx?paperid=86034)
- Thermal Conductivity Enhancement of Epoxy by Hybrid Particulate Fillers of Graphite and Silicon Carbide (paperinformation.aspx?paperid=54407)
- Detailed Micro Raman Spectroscopy Analysis of Doped Silicon Thin Film Layers and Its Feasibility for Heterojunction Silicon Wafer Solar Cells (paperinformation.aspx?paperid=38124)
- Analysis of Thermal Conductivity of Frost on Cryogenic Finned-tube Vaporizer Using Fractal Method (paperinformation.aspx?paperid=37886)

Figure A.6. Copyright permission for Figure 1.6.

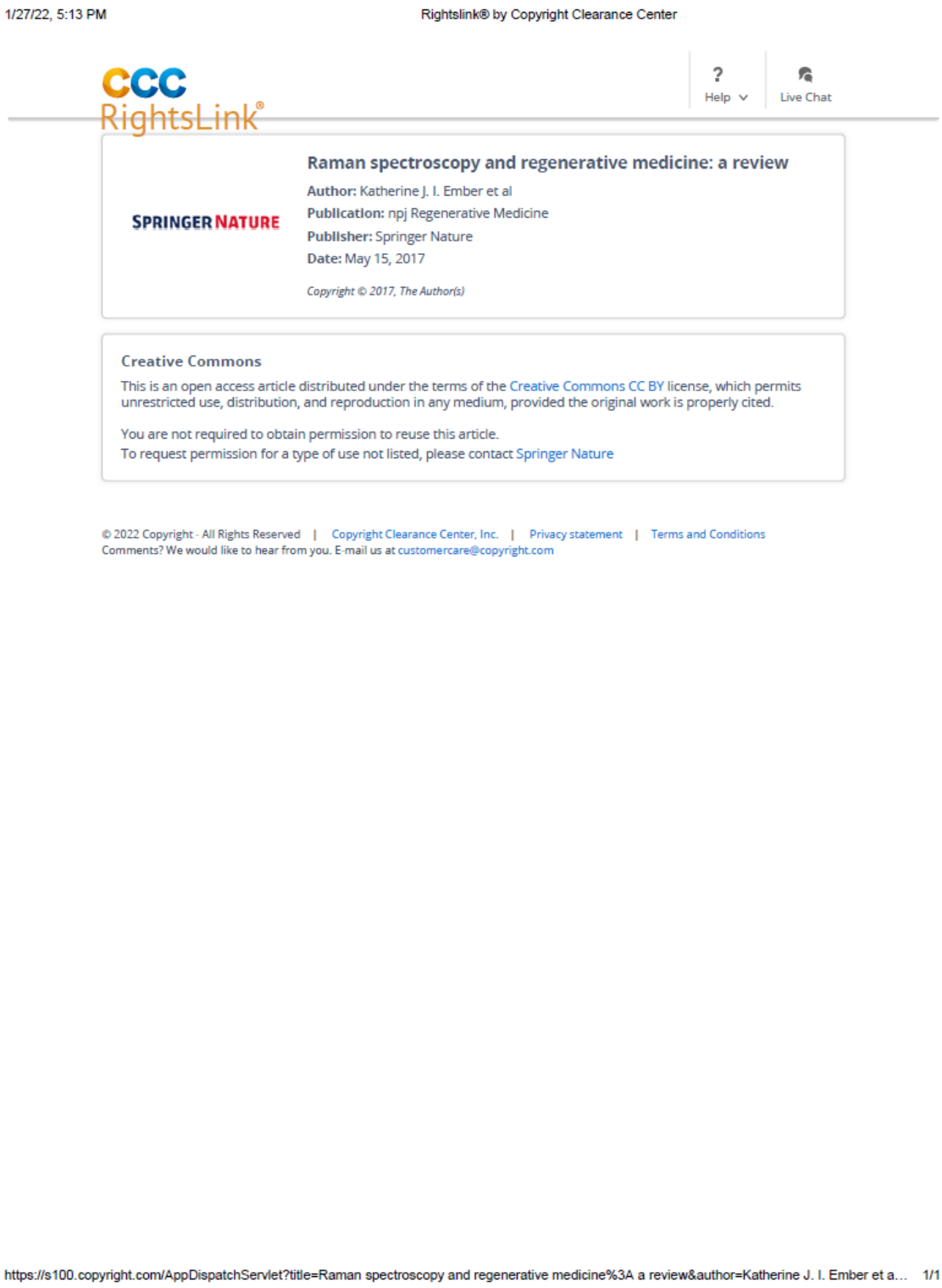


Figure A.7. Copyright permission for Figure 1.7.

AIP PUBLISHING LICENSE
TERMS AND CONDITIONS

Jan 27, 2022

This Agreement between Bogazici University -- Taher Meydando ("You") and AIP Publishing ("AIP Publishing") consists of your license details and the terms and conditions provided by AIP Publishing and Copyright Clearance Center.

License Number	5237030605177
License date	Jan 27, 2022
Licensed Content Publisher	AIP Publishing
Licensed Content Publication	Journal of Applied Physics
Licensed Content Title	Temperature-dependent Raman studies and thermal conductivity of direct CVD grown non-van der Waals layered Bi2O2Se
Licensed Content Author	Md Tarik Hossain, P. K. Giri
Licensed Content Date	May 7, 2021
Licensed Content Volume	129
Licensed Content Issue	17
Type of Use	Thesis/Dissertation
Requestor type	University or Educational Institution

Figure A.8. Copyright permission for Figure 1.8.

Format	Print and electronic
Portion	Figure/Table
Number of figures/tables	1
Will you be translating?	No
Title	Modified Numerical Method for Thin Film Thermal Conductivity Calculation with Micro-Raman Spectroscopy
Institution name	Bogazici University
Expected presentation date	Jan 2022
Order reference number	123123
Portions	Figure 7 (a) and (b)
Requestor Location	Bogazici University Bebek/Besiktas Istanbul, 34342 Turkey Attn: Bogazici University
Total	0.00 USD

Terms and Conditions

AIP Publishing -- Terms and Conditions: Permissions Uses

AIP Publishing hereby grants to you the non-exclusive right and license to use and/or distribute the Material according to the use specified in your order, on a one-time basis, for the specified term, with a maximum distribution equal to the number that you have ordered. Any links or other content accompanying the Material are not the subject of this license.

Figure A.8. Copyright permission for Figure 1.8 (cont.).

1. You agree to include the following copyright and permission notice with the reproduction of the Material:"Reprinted from [FULL CITATION], with the permission of AIP Publishing." For an article, the credit line and permission notice must be printed on the first page of the article or book chapter. For photographs, covers, or tables, the notice may appear with the Material, in a footnote, or in the reference list.
2. If you have licensed reuse of a figure, photograph, cover, or table, it is your responsibility to ensure that the material is original to AIP Publishing and does not contain the copyright of another entity, and that the copyright notice of the figure, photograph, cover, or table does not indicate that it was reprinted by AIP Publishing, with permission, from another source. Under no circumstances does AIP Publishing purport or intend to grant permission to reuse material to which it does not hold appropriate rights.
   You may not alter or modify the Material in any manner. You may translate the Material into another language only if you have licensed translation rights. You may not use the Material for promotional purposes.
3. The foregoing license shall not take effect unless and until AIP Publishing or its agent, Copyright Clearance Center, receives the Payment in accordance with Copyright Clearance Center Billing and Payment Terms and Conditions, which are incorporated herein by reference.
4. AIP Publishing or Copyright Clearance Center may, within two business days of granting this license, revoke the license for any reason whatsoever, with a full refund payable to you. Should you violate the terms of this license at any time, AIP Publishing, or Copyright Clearance Center may revoke the license with no refund to you. Notice of such revocation will be made using the contact information provided by you. Failure to receive such notice will not nullify the revocation.
5. AIP Publishing makes no representations or warranties with respect to the Material. You agree to indemnify and hold harmless AIP Publishing, and their officers, directors, employees or agents from and against any and all claims arising out of your use of the Material other than as specifically authorized herein.
6. The permission granted herein is personal to you and is not transferable or assignable without the prior written permission of AIP Publishing. This license may not be amended except in a writing signed by the party to be charged.
7. If purchase orders, acknowledgments or check endorsements are issued on any forms containing terms and conditions which are inconsistent with these provisions, such inconsistent terms and conditions shall be of no force and effect. This document, including the CCC Billing and Payment Terms and Conditions, shall be the entire agreement between the parties relating to the subject matter hereof.

This Agreement shall be governed by and construed in accordance with the laws of the State of New York. Both parties hereby submit to the jurisdiction of the courts of New York County for purposes of resolving any disputes that may arise hereunder.

V1.2

Questions? customercare@copyright.com or +1-855-239-3415 (toll free in the US) or +1-978-646-2777.

Figure A.8. Copyright permission for Figure 1.8 (cont.).

ELSEVIER LICENSE
TERMS AND CONDITIONS

Jan 27, 2022

This Agreement between Bogazici University -- Taher Meydando ("You") and Elsevier ("Elsevier") consists of your license details and the terms and conditions provided by Elsevier and Copyright Clearance Center.

License Number	5237030873237
License date	Jan 27, 2022
Licensed Content Publisher	Elsevier
Licensed Content Publication	Surface and Coatings Technology
Licensed Content Title	Adhesion and corrosion resistance of laser-oxidized titanium in potential biomedical application
Licensed Content Author	K.M. Łęcka,J. Gąsiorek,A. Mazur-Nowacka,B. Szczygieł,A.J. Antończak
Licensed Content Date	May 25, 2019
Licensed Content Volume	366
Licensed Content Issue	n/a
Licensed Content Pages	11
Start Page	179
End Page	189

Figure A.9. Copyright permission for Figure 4.14.

Type of Use	reuse in a thesis/dissertation
Portion	figures/tables/illustrations
Number of figures/tables/illustrations	1
Format	both print and electronic
Are you the author of this Elsevier article?	No
Will you be translating?	No
Title	Modified Numerical Method for Thin Film Thermal Conductivity Calculation with Micro-Raman Spectroscopy
Institution name	Bogazici University
Expected presentation date	Jan 2022
Order reference number	123123
Portions	Figure 1
Requestor Location	Bogazici University Bebek/Besiktas Istanbul, 34342 Turkey Attn: Bogazici University
Publisher Tax ID	GB 494 6272 12
Total	0.00 USD

Terms and Conditions

Figure A.9. Copyright permission for Figure 4.14 (cont.).

INTRODUCTION

1. The publisher for this copyrighted material is Elsevier. By clicking "accept" in connection with completing this licensing transaction, you agree that the following terms and conditions apply to this transaction (along with the Billing and Payment terms and conditions established by Copyright Clearance Center, Inc. ("CCC"), at the time that you opened your Rightslink account and that are available at any time at http://myaccount.copyright.com).

GENERAL TERMS

2. Elsevier hereby grants you permission to reproduce the aforementioned material subject to the terms and conditions indicated.

3. Acknowledgement: If any part of the material to be used (for example, figures) has appeared in our publication with credit or acknowledgement to another source, permission must also be sought from that source. If such permission is not obtained then that material may not be included in your publication/copies. Suitable acknowledgement to the source must be made, either as a footnote or in a reference list at the end of your publication, as follows:

"Reprinted from Publication title, Vol /edition number, Author(s), Title of article / title of chapter, Pages No., Copyright (Year), with permission from Elsevier [OR APPLICABLE SOCIETY COPYRIGHT OWNER]." Also Lancet special credit - "Reprinted from The Lancet, Vol. number, Author(s), Title of article, Pages No., Copyright (Year), with permission from Elsevier."

4. Reproduction of this material is confined to the purpose and/or media for which permission is hereby given.

5. Altering/Modifying Material: Not Permitted. However figures and illustrations may be altered/adapted minimally to serve your work. Any other abbreviations, additions, deletions and/or any other alterations shall be made only with prior written authorization of Elsevier Ltd. (Please contact Elsevier's permissions helpdesk here). No modifications can be made to any Lancet figures/tables and they must be reproduced in full.

6. If the permission fee for the requested use of our material is waived in this instance, please be advised that your future requests for Elsevier materials may attract a fee.

7. Reservation of Rights: Publisher reserves all rights not specifically granted in the combination of (i) the license details provided by you and accepted in the course of this licensing transaction, (ii) these terms and conditions and (iii) CCC's Billing and Payment terms and conditions.

8. License Contingent Upon Payment: While you may exercise the rights licensed immediately upon issuance of the license at the end of the licensing process for the transaction, provided that you have disclosed complete and accurate details of your proposed use, no license is finally effective unless and until full payment is received from you (either by publisher or by CCC) as provided in CCC's Billing and Payment terms and conditions. If full payment is not received on a timely basis, then any license preliminarily granted shall be deemed automatically revoked and shall be void as if never granted. Further, in the event that you breach any of these terms and conditions or any of CCC's Billing and Payment terms and conditions, the license is automatically revoked and shall be void as if never granted. Use of materials as described in a revoked license, as well as any use of the

Figure A.9. Copyright permission for Figure 4.14 (cont.).

materials beyond the scope of an unrevoked license, may constitute copyright infringement and publisher reserves the right to take any and all action to protect its copyright in the materials.

9. Warranties: Publisher makes no representations or warranties with respect to the licensed material.

10. Indemnity: You hereby indemnify and agree to hold harmless publisher and CCC, and their respective officers, directors, employees and agents, from and against any and all claims arising out of your use of the licensed material other than as specifically authorized pursuant to this license.

11. No Transfer of License: This license is personal to you and may not be sublicensed, assigned, or transferred by you to any other person without publisher's written permission.

12. No Amendment Except in Writing: This license may not be amended except in a writing signed by both parties (or, in the case of publisher, by CCC on publisher's behalf).

13. Objection to Contrary Terms: Publisher hereby objects to any terms contained in any purchase order, acknowledgment, check endorsement or other writing prepared by you, which terms are inconsistent with these terms and conditions or CCC's Billing and Payment terms and conditions. These terms and conditions, together with CCC's Billing and Payment terms and conditions (which are incorporated herein), comprise the entire agreement between you and publisher (and CCC) concerning this licensing transaction. In the event of any conflict between your obligations established by these terms and conditions and those established by CCC's Billing and Payment terms and conditions, these terms and conditions shall control.

14. Revocation: Elsevier or Copyright Clearance Center may deny the permissions described in this License at their sole discretion, for any reason or no reason, with a full refund payable to you. Notice of such denial will be made using the contact information provided by you. Failure to receive such notice will not alter or invalidate the denial. In no event will Elsevier or Copyright Clearance Center be responsible or liable for any costs, expenses or damage incurred by you as a result of a denial of your permission request, other than a refund of the amount(s) paid by you to Elsevier and/or Copyright Clearance Center for denied permissions.

LIMITED LICENSE

The following terms and conditions apply only to specific license types:

15. **Translation**: This permission is granted for non-exclusive world **English** rights only unless your license was granted for translation rights. If you licensed translation rights you may only translate this content into the languages you requested. A professional translator must perform all translations and reproduce the content word for word preserving the integrity of the article.

16. **Posting licensed content on any Website**: The following terms and conditions apply as follows: Licensing material from an Elsevier journal: All content posted to the web site must maintain the copyright information line on the bottom of each image; A hyper-text must be included to the Homepage of the journal from which you are licensing at http://www.sciencedirect.com/science/journal/xxxxx or the Elsevier homepage for books at http://www.elsevier.com; Central Storage: This license does not include permission for a scanned version of the material to be stored in a central repository such as that provided by Heron/XanEdu.

Figure A.9. Copyright permission for Figure 4.14 (cont.).

Licensing material from an Elsevier book: A hyper-text link must be included to the Elsevier homepage at http://www.elsevier.com . All content posted to the web site must maintain the copyright information line on the bottom of each image.

Posting licensed content on Electronic reserve: In addition to the above the following clauses are applicable: The web site must be password-protected and made available only to bona fide students registered on a relevant course. This permission is granted for 1 year only. You may obtain a new license for future website posting.

17. **For journal authors:** the following clauses are applicable in addition to the above:

Preprints:

A preprint is an author's own write-up of research results and analysis, it has not been peer-reviewed, nor has it had any other value added to it by a publisher (such as formatting, copyright, technical enhancement etc.).

Authors can share their preprints anywhere at any time. Preprints should not be added to or enhanced in any way in order to appear more like, or to substitute for, the final versions of articles however authors can update their preprints on arXiv or RePEc with their Accepted Author Manuscript (see below).

If accepted for publication, we encourage authors to link from the preprint to their formal publication via its DOI. Millions of researchers have access to the formal publications on ScienceDirect, and so links will help users to find, access, cite and use the best available version. Please note that Cell Press, The Lancet and some society-owned have different preprint policies. Information on these policies is available on the journal homepage.

Accepted Author Manuscripts: An accepted author manuscript is the manuscript of an article that has been accepted for publication and which typically includes author-incorporated changes suggested during submission, peer review and editor-author communications.

Authors can share their accepted author manuscript:

- immediately
  - via their non-commercial person homepage or blog
  - by updating a preprint in arXiv or RePEc with the accepted manuscript
  - via their research institute or institutional repository for internal institutional uses or as part of an invitation-only research collaboration work-group
  - directly by providing copies to their students or to research collaborators for their personal use
  - for private scholarly sharing as part of an invitation-only work group on commercial sites with which Elsevier has an agreement
- After the embargo period
  - via non-commercial hosting platforms such as their institutional repository
  - via commercial sites with which Elsevier has an agreement

In all cases accepted manuscripts should:

- link to the formal publication via its DOI
- bear a CC-BY-NC-ND license - this is easy to do
- if aggregated with other manuscripts, for example in a repository or other site, be shared in alignment with our hosting policy not be added to or enhanced in any way to

Figure A.9. Copyright permission for Figure 4.14 (cont.).

appear more like, or to substitute for, the published journal article.

Published journal article (JPA): A published journal article (PJA) is the definitive final record of published research that appears or will appear in the journal and embodies all value-adding publishing activities including peer review co-ordination, copy-editing, formatting, (if relevant) pagination and online enrichment.

Policies for sharing publishing journal articles differ for subscription and gold open access articles:

Subscription Articles: If you are an author, please share a link to your article rather than the full-text. Millions of researchers have access to the formal publications on ScienceDirect, and so links will help your users to find, access, cite, and use the best available version.

Theses and dissertations which contain embedded PJAs as part of the formal submission can be posted publicly by the awarding institution with DOI links back to the formal publications on ScienceDirect.

If you are affiliated with a library that subscribes to ScienceDirect you have additional private sharing rights for others' research accessed under that agreement. This includes use for classroom teaching and internal training at the institution (including use in course packs and courseware programs), and inclusion of the article for grant funding purposes.

Gold Open Access Articles: May be shared according to the author-selected end-user license and should contain a CrossMark logo, the end user license, and a DOI link to the formal publication on ScienceDirect.

Please refer to Elsevier's posting policy for further information.

18. **For book authors** the following clauses are applicable in addition to the above: Authors are permitted to place a brief summary of their work online only. You are not allowed to download and post the published electronic version of your chapter, nor may you scan the printed edition to create an electronic version. **Posting to a repository:** Authors are permitted to post a summary of their chapter only in their institution's repository.

19. **Thesis/Dissertation**: If your license is for use in a thesis/dissertation your thesis may be submitted to your institution in either print or electronic form. Should your thesis be published commercially, please reapply for permission. These requirements include permission for the Library and Archives of Canada to supply single copies, on demand, of the complete thesis and include permission for Proquest/UMI to supply single copies, on demand, of the complete thesis. Should your thesis be published commercially, please reapply for permission. Theses and dissertations which contain embedded PJAs as part of the formal submission can be posted publicly by the awarding institution with DOI links back to the formal publications on ScienceDirect.

Elsevier Open Access Terms and Conditions

You can publish open access with Elsevier in hundreds of open access journals or in nearly 2000 established subscription journals that support open access publishing. Permitted third party re-use of these open access articles is defined by the author's choice of Creative Commons user license. See our open access license policy for more information.

Terms & Conditions applicable to all Open Access articles published with Elsevier:

Figure A.9. Copyright permission for Figure 4.14 (cont.).

Any reuse of the article must not represent the author as endorsing the adaptation of the article nor should the article be modified in such a way as to damage the author's honour or reputation. If any changes have been made, such changes must be clearly indicated.

The author(s) must be appropriately credited and we ask that you include the end user license and a DOI link to the formal publication on ScienceDirect.

If any part of the material to be used (for example, figures) has appeared in our publication with credit or acknowledgement to another source it is the responsibility of the user to ensure their reuse complies with the terms and conditions determined by the rights holder.

Additional Terms & Conditions applicable to each Creative Commons user license:

CC BY: The CC-BY license allows users to copy, to create extracts, abstracts and new works from the Article, to alter and revise the Article and to make commercial use of the Article (including reuse and/or resale of the Article by commercial entities), provided the user gives appropriate credit (with a link to the formal publication through the relevant DOI), provides a link to the license, indicates if changes were made and the licensor is not represented as endorsing the use made of the work. The full details of the license are available at http://creativecommons.org/licenses/by/4.0.

CC BY NC SA: The CC BY-NC-SA license allows users to copy, to create extracts, abstracts and new works from the Article, to alter and revise the Article, provided this is not done for commercial purposes, and that the user gives appropriate credit (with a link to the formal publication through the relevant DOI), provides a link to the license, indicates if changes were made and the licensor is not represented as endorsing the use made of the work. Further, any new works must be made available on the same conditions. The full details of the license are available at http://creativecommons.org/licenses/by-nc-sa/4.0.

CC BY NC ND: The CC BY-NC-ND license allows users to copy and distribute the Article, provided this is not done for commercial purposes and further does not permit distribution of the Article if it is changed or edited in any way, and provided the user gives appropriate credit (with a link to the formal publication through the relevant DOI), provides a link to the license, and that the licensor is not represented as endorsing the use made of the work. The full details of the license are available at http://creativecommons.org/licenses/by-nc-nd/4.0. Any commercial reuse of Open Access articles published with a CC BY NC SA or CC BY NC ND license requires permission from Elsevier and will be subject to a fee.

Commercial reuse includes:

- Associating advertising with the full text of the Article
- Charging fees for document delivery or access
- Article aggregation
- Systematic distribution via e-mail lists or share buttons

Posting or linking by commercial companies for use by customers of those companies.

20. **Other Conditions**:

v1.10

Figure A.9. Copyright permission for Figure 4.14 (cont.).

Questions? customercare@copyright.com or +1-855-239-3415 (toll free in the US) or +1-978-646-2777.

Figure A.9. Copyright permission for Figure 4.14 (cont.).